

# Nuclear Field Theory predictions for $^{11}\text{Li}$ and $^{12}\text{Be}$ : shedding light on the origin of pairing in nuclei

G. Potel,<sup>1,2</sup> A. Idini,<sup>3,4</sup> F. Barranco,<sup>5</sup> E. Vigezzi,<sup>4</sup> and R.A. Broglia<sup>3,4,6</sup>

<sup>1</sup>*Departamento de Física Atomica, Molecular y Nuclear,*

*Universidad de Sevilla, Facultad de Física, Avda. Reina Mercedes s/n, Spain.*

<sup>2</sup>*CEA-Saclay, DSM/IRFU/SPhN, F-91191 Gif-sur-Yvette, France (Present Address)*

<sup>3</sup>*Department of Physics, University of Milano, via Celoria 16, 20133 Milan, Italy*

<sup>4</sup>*INFN, Milan Section, via Celoria 16, 20133 Milan, Italy*

<sup>5</sup>*Departamento de Física Aplicada III, Universidad de Sevilla,*

*Escuela Superior de Ingenieros, Sevilla,*

*41092 Camino de los Descubrimientos s/n, Spain.*

<sup>6</sup>*The Niels Bohr Institute, University of Copenhagen,*

*Blegdamsvej 17, DK-2100 Copenhagen, Denmark*

(December 12, 2012)

Recent data resulting from studies of two-nucleon transfer reaction on  $^{11}\text{Li}$ , analyzed through a unified nuclear-structure-direct-reaction theory have provided strong direct as well as indirect confirmation, through the population of the first excited state of  $^9\text{Li}$  and of the observation of a strongly quenched ground state transition, of the prediction that phonon mediated pairing interaction is the main mechanism binding the neutron halo of the 8.5 ms-lived  $^{11}\text{Li}$  nucleus. In other words, the ground state of  $^{11}\text{Li}$  can be viewed as a neutron Cooper pair bound to the  $^9\text{Li}$  core, mainly through the exchange of collective vibration of the core and of the pigmy resonance arising from the sloshing back and forth of the neutron halo against the protons of the core, the mean field leading to unbound two particle states, a situation essentially not altered by the bare nucleon-nucleon interaction acting between the halo neutrons. Two-neutron pick-up data, together with  $(t, p)$  data on  $^7\text{Li}$ , suggest the existence of a pairing vibrational band based on  $^9\text{Li}$ , whose members can be excited with the help of inverse kinematic experiments as was done in the case of  $^{11}\text{Li}(p, t)^9\text{Li}$  reaction. The deviation from harmonicity can provide insight

into the workings of medium polarization effects on Cooper pair nuclear pairing, let alone specific information concerning the “rigidity” of the  $N=6$  shell closure. Further information concerning these questions is provided by the predicted absolute differential cross sections  $\sigma_{abs}$  associated with the reactions  $^{12}\text{Be}(p,t)^{10}\text{Be}(\text{gs})$  and  $^{12}\text{Be}(p,t)^{10}\text{Be}(pv)(\approx^{10}\text{Be}(p,t)^8\text{Be}(\text{gs}))$ . In particular, concerning this last reaction, predictions of  $\sigma_{abs}$  can change by an order of magnitude depending on whether the halo properties associated with the  $d_{5/2}$  orbital are treated selfconsistently in calculating the ground state correlations of the (pair removal) mode, or not.

## I. INTRODUCTION

At the basis of BCS theory of superconductivity one finds the condensation of strongly overlapping Cooper pairs. This model can be extended to the atomic nucleus, provided one takes pair fluctuations into account, fluctuations which renormalize in an important way the different quantities entering the theory, in particular the pairing gap ( $\Delta = (\Delta_{\text{BCS}}^2 + \Delta_{\text{Fluct}}^2)^{1/2}$ , see e.g. [1] Fig. 6.2 p. 152 and connected discussion). Not only pairing vibrations are more collective in the nuclear case than in condensed matter (see e.g. [2]) and in liquid  $^3\text{He}$  [3], where they essentially correspond to a two quasiparticle-like state lying on top of twice the pairing gap. They also develop, in the nuclear case, as well defined vibrational bands around closed shell nuclei, where one can clearly distinguish between particle and hole degrees of freedom, in keeping with the relatively large gap existing between occupied and unoccupied single-particle states. Systematic evidence exists of the correlation and stability of the pair addition and pair subtraction modes (single Cooper pairs) in medium heavy nuclei (see e.g. [1] and [4] and references therein). Making use of these building blocks a number of pairing vibrational bands have been identified, providing important insight into the mechanism in which nuclear superfluidity emerges from the condensation of many phonon pairing modes. In medium heavy nuclei, a large fraction of the pairing correlation energy ( $\gtrsim 50\text{--}70\%$ ) is due to the strong  $^1\text{S}_0$   $N\text{--}N$  bare interaction, medium polarization effects being important although not dominant (see [5] as well as [1], Ch. 10 and refs. therein). This is, among other things, one of the reasons why the multi-phonon pairing spectra seen to date are rather harmonic (see e.g. [6]). In other words, the interaction between pairing modes in heavy stable nuclei is weak and anharmonicities effects are, although very revealing of the

nuclear structure around closed shell nuclei, not very important (note however Pauli principle effects [7]).

We expect the situation to be rather different in the case of weakly bound, strongly polarizable light halo nuclei like  $^{11}\text{Li}$  and, to some extent also  $^{12}\text{Be}$ . In both cases, the N–N bare interaction provides a small contribution ( $\approx 100$  keV) to the two-neutron binding energy. Thus a major fraction of the glue holding the neutron Cooper pair (halo) to the  $^9\text{Li}$  and to the  $^{10}\text{Be}$  cores arises from the exchange of collective vibrations [8, 9]. To further clarify the origin of pairing in nuclei, it would then be important to look for the pairing vibrational band associated with the  $N = 6$  closed shell systems  $^9\text{Li}$  and  $^{10}\text{Be}$ . Larger or smaller anharmonicities as compared with other closed shell systems (like e.g.  $^{208}\text{Pb}$ ) would provide a welcome input to shed light on the relative contributions to the nuclear pairing force, both in terms of the strength as well as of the radial shape (form-factors), of the bare  $N$ – $N$  force and of the effective pairing force arising from the exchange of collective vibrations between pairs of nucleons moving in time reversal states close to the Fermi energy. In fact, if all of the  $^1\text{S}_0$  correlations came from the short range, bare interaction, many processes leading to anharmonic effects would not be present in the pairing vibrational nuclear spectrum. In particular, a special group of those related to Pauli principle corrections reflecting the overcompleteness of the NFT basis of elementary excitations, i.e. single-particle, particle-hole-like and pair vibrational modes.

## II. NUCLEAR FIELD THEORY

Nuclear Field Theory (NFT) provides a systematic method for describing both nuclear structure [10–16] and nuclear reactions [17]. In particular, it allows to deal with the problem of overcompleteness of the degrees of freedom arising from the identity of particles appearing explicitly and the particles participating in the collective motion. The non-orthogonality of the variety of degrees of freedom must be expected quite generally in descriptions that: a) from the nuclear structure point of view exploit simultaneously the single-particle degrees of freedom, as well as the quanta of particle–hole type together with those involving pairing vibrations [18] made out of two correlated particles (pair addition modes) or of two correlated holes (pair subtraction modes); b) from the reaction point of view, make use of mean fields of target and of projectile which are assumed to be independent of each other, with the added

possibility, in the case of the study of pairing correlations through two-particle transfer reactions, that a member of a Cooper pair [19], [20] is in one system (e.g. target) and the second partner in the other one (i.e. projectile). This is in keeping with the fact that the typical value of the pairing gap in superfluid nuclei (or of correlation energies in the case of normal systems) is  $\Delta \approx 1$  MeV, implying that Cooper pair partners are correlated over distances of the order of the associated coherence length,  $\xi \approx 20\text{-}30$  fm. This result, together with the fact that  $\Delta/U(r \approx R_0) \approx 4 \times 10^{-2}$ ,  $U(r)$  being the average mean field potential, implies, as a rule, that successive transfer, where  $U$  acts twice, is dominant as compared to the simultaneous transfer of two nucleons, a process in which  $U$  acts once, the second nucleon being transferred partially making use of the interaction energy between the partners of the Cooper pair, and partially exploiting the non-orthogonality of the single-particle wavefunctions associated with the mean field of target and projectile. It is of notice that this argumentation is at the basis of one of the cornerstones of superconductivity in metals, namely the Josephson effect [21, 22] (see also [23] and references therein).

Tailored after Feynman's version of Quantum Electrodynamics (QED) [24], that is in terms of Feynman diagrams, NFT is essentially only restricted by the limitations in the (experimental) knowledge one has of the particle-vibration coupling vertices  $\Lambda_\alpha(\beta)$ , where  $\alpha$  indicates the quantum numbers of the phonon but associated with gauge space, as well as whether the mode in consideration is the first, second, etc. in energy, while  $\beta = 0, \pm 2$ , is the transfer quantum number ( $\beta = 0$  implies particle-hole excitations, while  $\beta = +2$  pair-addition and  $\beta = -2$  pair-removal modes respectively, see e.g. [4], [15] and [25] and refs. therein). At variance with QED for which an essentially definitive value of the fine structure constant  $e^2/\hbar c$  exists, uncertainties are to be ascribed to the variety of  $\Lambda_\alpha(\beta)$  values. This is due to the combined effect of the fragmentation of the modes, as well as the fact that to extract  $\Lambda_\alpha(\beta)$  from a reaction measurement one needs to use optical potentials, with all the associated limitations of such an approach (see Fig. 1).

In any case, progress which has taken place during recent years has ushered studies of nuclear pairing with two-nucleon transfer reactions into the quantitative era, with uncertainties well within experimental errors (see e.g. [26–29] and refs. therein).

### III. THE COOPER PAIR PROBLEM AND $^{11}\text{Li}$

The basis for the understanding of superconductivity in metals worked out by Bardeen, Cooper and Schrieffer (BCS theory [30]) was provided by Cooper [19] who solved the problem of a pair of electrons interacting above a noninteracting Fermi sea of electrons via a two-body potential.  $^{11}\text{Li}$  can be viewed as a rather accurate realization of Cooper's model, within the framework of nuclear physics: a pair of neutrons weakly bound to the  $^9\text{Li}$  core.

Now, it was found in a NFT study of this halo nucleus [8], that the bare nucleon–nucleon interaction does not bind the Cooper pair (see Fig. 2 (a)). It is the exchange of the vibrations of the halo field and of the core (dipole and quadrupole) between the halo neutrons which, similar to phonons in metals, binds the Cooper pair (see Fig. 2 (b)). The NFT results of ref. [8] provide a rather accurate description of the nuclear structure properties of  $^{11}\text{Li}$ . The calculations were carried out following all what is well known about NFT and the particle–vibration coupling mechanism (see, e.g. [10–16], [25] and refs. therein). A single mean field potential (Saxon–Woods) was used for all single-particle ( $s$ –,  $p$ –,  $d$ –, ...) states (cf. [31] pp. 236–240). Parity inversion of the  $s_{1/2}$  and  $p_{1/2}$  states of  $^{10}\text{Li}$  results from the coupling of these resonances to vibrations of the  $^9\text{Li}$  core <sup>1</sup>, when the coupling to the continuum is taken properly into account. Making use of the resulting single-particle (dressed) states, of the bare N–N interaction and of the interaction induced by the exchange of collective modes between the dressed single-particle halo states, including the  $1^-$  pigmy resonance of  $^{11}\text{Li}$  (cf. Fig. 2 (b)), a quantitative account of the experimental findings was obtained, in particular concerning the extremely low two-neutron separation energy  $S_{2n} \approx 0.38$  MeV [32, 33] (see also Caption to Fig. 2). Notice that if the  $N$ – $N$  interaction is not included, the absolute value of  $S_{2n}$  is decreased by only about 100 keV.

The NFT description of the structure of  $^{11}\text{Li}$  also contained precise predictions (see e.g. [1] Ch. 11, in particular Fig. 11.6) concerning how to force virtual correlation processes, to become real. Namely, through two-neutron pick-up reactions, like e.g.  $^{11}\text{Li}(p, t)^9\text{Li}$ . In this way it was found that one can excite, among others, the multiplet of states  $(2^+ \otimes p_{3/2}(\pi))_{1/2^-, 3/2^-, 5/2^-, 7/2^-}$  (see Fig. 2 (c), see also Figs. 3 and 4). These predictions had to wait short of ten years to be tested (see ref. [34]), and proved not to be wrong. <sup>2</sup> In fact,

<sup>1</sup> Of notice that this is tantamount to saying of the  $^8\text{He}$  core, in keeping with the fact that the  $p_{3/2}$  proton state is considered throughout as a spectator.

<sup>2</sup> First we guess it. Then we compute the consequences of the guess to see what would be implied if the

making use of a detailed nuclear reaction theory of two-particle transfer which considers successive, simultaneous and non-orthogonality processes, together with inelastic and break up channels and thus accurately treats the coupling to the continuum concerning both the structure and reaction aspects of the calculations, one has been able [26] to check the validity of such predictions, and reproduce in a quantitative fashion, the experimental findings of ref. [34]. In particular the observation of the  $1/2^-$  member of the  $(2^+ \otimes p_{3/2}(\pi))$  multiplet of  $^9\text{Li}$  which is the first excited state of this nucleus (see Fig. 4). This result provided the first, direct confirmation of the central role played by vibrational states in nuclear pairing.

#### IV. PAIRING VIBRATIONAL BAND OF $^9\text{Li}$

The unified NFT description of structure and reactions used in refs. [8, 26], provides a number of suggestions concerning the consequences the findings reported in [34] has. In particular, the existence of a many-phonon pair vibrational spectrum (see Fig. 5), similar to that observed in  $(p, t)$  and  $(t, p)$  reactions in the Pb region<sup>3</sup> (see e.g. [1, 4, 6]).

The energy of the two-phonon state ( $n_a = 1, n_r = 1$ ) mode of  $^9\text{Li}$ , where  $n_i$  indicates the number of pair addition ( $i = a$ ; ground state of  $^{11}\text{Li}$ ) and pair removal ( $i = r$ ; ground state of  $^7\text{Li}$ ) modes is expected to be, in the harmonic approximation [18] (see also App. A),

$$\begin{aligned} W(n_r = 1; n_a = 1) &= (B(9) - B(7)) - (B(11) - B(9)) \\ &= (45.34 - 39.25) - (45.71 - 45.34) \text{ MeV} = (6.1 - 0.4) \text{ MeV} = 5.7 \text{ MeV} \\ &= W_1(\beta = 2) + W_1(\beta = -2), \end{aligned} \quad (1)$$

where  $B(A)$  is the binding energy of the Li-isotope with mass number  $A$  (see Fig.6, see also App. A and Fig. 21 below).

The excitation energy of a state of the vibrational band (again in the harmonic approximation), can be written as

$$W(n_r, n_a) = n_r W_1(\beta = -2) + n_a W_1(\beta = 2). \quad (2)$$

---

law we guess is right. Then we compare the result of the computation to nature, with experiment or experience, compare it directly with observation, to see if it works. If it disagrees with experiment it is wrong. In that simple statement is the key to science. It does not make any difference how beautiful your guess is. It does not make any difference how smart you are, who made the guess, or what your name is.

If it disagrees with experiment it is wrong. That is all there is to it. Richard Feynman

<sup>3</sup> The main expected difference concerns the relative importance of the bare and induced interaction which binds the Cooper neutron pair to the core, namely to  $^{208}\text{Pb}$  in one case and  $^9\text{Li}$  in the other. An important consequence of this difference is to be related with the expected anharmonicities of the halo pairing vibrational spectrum.

The absolute value of the different transitions between these states can be expressed in terms of the basic cross-sections

$$a = \sigma \left( {}^9\text{Li}(gs) \leftrightarrow {}^{11}\text{Li}(gs) \right) \quad \text{and} \quad r = \sigma \left( {}^9\text{Li}(gs) \leftrightarrow {}^7\text{Li}(gs) \right) . \quad (3)$$

An embodiment of the above definitions is provided by the values [34, 35] (see also [36]),

$$a = d\sigma \left( {}^{11}\text{Li}(p, t) {}^9\text{Li}(gs); \theta = 60^\circ \right) / d\Omega = 0.7 \text{ mb/sr}, \quad (4)$$

and

$$r = d\sigma \left( {}^7\text{Li}(t, p) {}^9\text{Li}(gs); \theta = 60^\circ \right) / d\Omega = 3 \text{ mb/sr}, \quad (5)$$

and the principle of detailed balance. It is of notice that while  $W_1(\beta = 2)$  and  $W_1(\beta = -2)$  are intrinsic properties of the pairing vibrational modes (it is reminded that the Fermi energy within the framework of the pairing vibrational model is determined by the value of the energy associated with the minimum of the RPA dispersion relation, see Apps. A and C), (4) and (5) depend also on the bombarding conditions (bombarding energy, scattering angle, etc), as well as on the reaction  $((p, t), ({}^{18}\text{O}, {}^{16}\text{O}), \text{etc})$ . Within this context it is of notice that the values reported in (4) and (5) corresponds to tritons of  $\sim 3$  MeV and of 5 MeV per nucleon respectively (see also App. D).

With such caveat in mind one expects that (see also [6]), at equal bombarding conditions as those corresponding to (4) and (5) (see [34, 35])

$$d\sigma \left( {}^{11}\text{Li}(t, p) {}^{13}\text{Li}(gs); \theta = 60^\circ \right) / d\Omega \approx 1.4 \text{ mb/sr}, \quad (6)$$

and

$$d\sigma \left( {}^7\text{Li}(p, t) {}^5\text{Li}(gs); \theta = 60^\circ \right) / d\Omega \approx 6 \text{ mb/sr}, \quad (7)$$

in a similar way in which the transition  $\left( \begin{smallmatrix} 2^+ \\ \text{phonon} \end{smallmatrix} \otimes \begin{smallmatrix} 2^+ \\ \text{phonon} \end{smallmatrix} \right) \rightarrow \left( \begin{smallmatrix} 2^+ \\ \text{phonon} \end{smallmatrix} \right)$  is expected to display a  $B(E2)$ -value twice as large as that associated with the transition of the one phonon state to the ground state i.e.  $\left( \begin{smallmatrix} 2^+ \\ \text{phonon} \end{smallmatrix} \right) \rightarrow (gs)$ .

In Fig. 5 the one- and two-phonon quadrupole spectrum of  ${}^9\text{Li}$  expected in the harmonic approximation is also shown. In Fig. 6 we display the pairing vibrational spectrum of  ${}^9\text{Li}$  and the associated absolute two-particle transfer differential cross sections of the pair addition and pair removal modes, in comparison with the experimental data [34],[35].

In the case of the reaction  $^{11}\text{Li}(p, t)^9\text{Li}(\text{gs})$  the absolute differential cross section was calculated making use of the two-nucleon spectroscopic amplitudes obtained from the  $|0\rangle$  term of the neutron component of the  $^{11}\text{Li}$  ground state ( $\equiv |\tilde{0}\rangle_\nu \otimes |p_{3/2}(\pi)\rangle$ , cf. [28]),

$$|\tilde{0}\rangle_\nu = |0\rangle + \alpha|(p_{1/2}, s_{1/2})_{1-} \otimes 1^-; 0\rangle + \beta|(s_{1/2}, d_{5/2})_{2+} \otimes 2^+; 0\rangle, \quad (8)$$

with  $\alpha = 0.7$  and  $\beta \approx 0.1$ , and

$$|0\rangle = 0.45|s_{1/2}^2(0)\rangle + 0.55|p_{1/2}^2(0)\rangle + 0.04|d_{5/2}^2(0)\rangle, \quad (9)$$

describing the motion of the two halo neutrons around  $^9\text{Li}$ . Successive, simultaneous and non-orthogonality contributions to the two-particle transfer process were taken into account (see [26, 29, 34] and refs. therein). The optical parameters used to describe the  $^{11}\text{Li}+p$ ,  $^{10}\text{Li}+d$  and the  $^9\text{Li}+t$  channels were taken from refs. [34], [37].

In the case of  $^7\text{Li}(t, p)^9\text{Li}(\text{gs})$  reaction, the optical parameters were taken from refs. [35], [37] while the two-neutron spectroscopic amplitudes, reported in Table I, were calculated within the RPA (cf. e.g. [1] and [4], see App. A), making use of a Saxon-Woods potential with standard parametrization (see [31] pp. 236-240) to describe the single-particle energies, and of the experimental correlation energy of the two-neutron holes in  $^7\text{Li}(\text{gs})$  (as an example (in this case regarding Be-isotopes), cf. Caption to Fig. 23). As seen from Fig. 6 and Table II, theory provides an overall account of the experimental findings. While it is the component (9) which is directly involved in the  $^{11}\text{Li}(p, t)^9\text{Li}(\text{gs})$  transfer process, the amplitudes  $\alpha$  and  $\beta$  play a central role concerning the absolute value of the cross section. In fact, incorrectly normalizing the state (9) to 1, that is  $0.63|s_{1/2}^2(0)\rangle + 0.77|p_{1/2}^2(0)\rangle + 0.06|d_{5/2}^2(0)\rangle$ , leads to an integrated cross section in the angular range  $20^\circ - 150^\circ$  of 12.1 mb. This result is a factor of 2 larger than that predicted making use of (9), and lies outside the errors of the experimental value  $\sigma_{exp} = 5.7 \pm 0.9$  (see Table II as well as [26] and [34]); see also Fig. 7(a), result labeled TDA).

Within this context, one can also play the same game concerning the two-nucleon spectroscopic amplitudes associated with the reaction  $^7\text{Li}(t, p)^9\text{Li}(\text{gs})$ , by setting  $Y_1^r(k) = 0$  and normalizing the RPA pair removal wavefunction according to  $\sum_i (X_1^r(i))^2 = 1$ . In other words, neglecting ground state correlations (TD approximation) which leads to  $X_1^r(s_{1/2}) = 0.055$  and  $X_1^r(p_{3/2}) = 0.998$ . The resulting absolute cross section for the reaction  $^7\text{Li}(t, p)^9\text{Li}(\text{gs})$  integrated in the range  $10^\circ - 109^\circ$  becomes 9.1 mb, a value which lies outside the experimental errors of the observed value (see Table II and Fig. 7 (b)).



As shown in Figs. 8 and 9, anharmonicities in the pairing vibrational spectrum can arise due to a number of physical effects. For example: 1) Overcompleteness (see Fig. 9 (b) and (c)); 2) Pauli principle correction to multiphonon states (see e.g. Figs. 8(a), 8(b) and 9 (c)) leading, in connection with phonon mediated pairing (see e.g. Fig. 8(b)), to correlation (CO)-like processes [38] (see inset (a) of Fig. 10). Within this context, it is of notice that the parity inversion observed to take place between the  $s_{1/2}$  and  $p_{1/2}$  states of a number of  $N = 7$  isotones (see Fig.10) is due, to a large extent, to CO processes [8, 9] (see inset (a) in Fig. 10). This is in keeping with the fact that among the largest components of the  $2^+$  vibration of  $^8\text{He}$  and of  $^{10}\text{Be}$  one finds the  $(1p_{1/2}, 1p_{3/2}^{-1})$  particle-hole component.

It is then expected that the contributions to the anharmonicity of the pairing vibrational band in light halo nuclei (like  $^{11}\text{Li}$  but also  $^{12}\text{Be}$ , see Sect. V), can be important, in keeping with the high polarizability displayed by these systems as compared with, for example,  $^{208}\text{Pb}$ . The energy of the two-phonon pairing vibrational mode given in Fig. 6 for  $^9\text{Li}$  (as well as that associated with  $^{10}\text{Be}$ , see Sect. V below) could, in principle, be strongly modified by such effects, as well as by coupling to states consisting of two (particle-hole-like) phonons (see Fig. 9(c); within this connection see [39] as well as App. B).

### A. The optical potential

In keeping with the fact that structure and reactions are just but two aspects of the same physics and that in the study of light halo nuclei, continuum states are to be treated on, essentially, equal footing in the calculation of the wavefunctions describing bound states (**structure**) as well as of the asymptotic distorted waves entering in the calculation of the absolute two-particle transfer differential cross sections (reaction; see Figs. 11 (a) and 11 (b)), the calculation of the optical potentials is essentially within reach (**reaction**, see Fig. 11 (c) and Fig.12, see also e.g. [40, 41] and refs. therein).

Because the real and imaginary parts of complex functions are related by simple dispersion relations (see e.g. [38] and refs. therein) it is sufficient to calculate only one of the two (real or imaginary) components of the self-energy function to obtain the full scattering, complex, nuclear dielectric function (optical potentials). Now, absorption is controlled by on-the-energy shell contributions. Within this scenario it is likely that the simplest way to proceed is that of calculating the absorptive potential and then obtain the real part by dispersion

(see e.g. [42], [43]; see also [17]). Of notice that in heavy ion reactions, one is dealing with leptodermous systems. Thus, the real part of the optical potential can, in principle, be obtained by convolution of the nuclear densities and of the surface tension (see e.g. [17] and refs therein).

Within the present context, one can mention the ambiguities encountered in trying to properly define a parentage coefficient relating the system of  $(A + 1)$  nucleons to the system of  $A$  nucleons, and thus a spectroscopic amplitude (see e.g. [44, 45], see also [38]). In other words, a prefactor which allows to express the absolute one-particle transfer differential cross section in terms of the elastic cross section.

Making use of NFT diagrams like the one shown in Fig. 12, it is possible to calculate, one at a time, the variety of contributions leading to one- and two-particle transfer processes (in connection with this last one see Fig. 11). Summing up the different contributions, taking also proper care of those arising from four-point vertex, tadpole processes, etc. (see refs. [10–16] and refs. therein, see also [44]), a consistent description of the different channels can be worked out, in which the predicted quantities to be directly compared with observables are absolute differential cross sections, or, more generally, absolute values of strength functions for different scattering angles.

## V. THE PAIRING VIBRATIONAL SPECTRUM OF $^{10}\text{Be}$

Calculations similar to the ones discussed in previous sections have been carried out in connection with the expected  $N = 6$  shell closure pairing vibrational band of  $^{10}\text{Be}$ . In Fig. 13 we display the associated pairing vibrational spectrum in the harmonic approximation (see App. A, in particular section *b* of this Appendix). Also given are the absolute two-nucleon transfer differential cross sections associated with the excitation of the one-phonon pair addition and pair subtraction modes excited in the reactions  $^{12}\text{Be}(\text{p},\text{t})^{10}\text{Be}(\text{gs})$  and  $^{10}\text{Be}(\text{p},\text{t})^8\text{Be}(\text{gs})$  respectively, calculated for a bombarding energy appropriate for planned studies making use of inverse kinematic techniques [46].

The ((2p-2h)-like) two-phonon pairing vibration state of  $^{10}\text{Be}$  is expected, in this approximation, to lie at 4.8 MeV, equal to the sum of the energies of the pair removal  $W_1(\beta = -2) = 0.5$  MeV and of the pair addition  $W_1(\beta = 2) = 4.3$  MeV modes. In keeping with the fact that the lowest known  $0^+$  excited state of  $^{10}\text{Be}$  appears at about 6 MeV [47], we have used this

excitation energy in the calculation of the  $Q$ -value associated with the  $^{12}\text{Be}(p,t)^{10}\text{Be}(pv)$  cross section. The associated shift in energy from the harmonic value of 4.8 MeV can, arguably, be connected with anharmonicities of the  $^{10}\text{Be}$  pairing vibrational spectrum, as discussed in the case of  $^{11}\text{Li}$  in connection with Figs. 8 and 9. Medium polarization effects (see e.g. Fig. 8(b)) may also lead to conspicuous anharmonicities in the pairing vibrational spectrum.

The two-nucleon spectroscopic amplitudes corresponding to the reaction  $^{10}\text{Be}(p,t)^8\text{Be}(\text{gs})$  and displayed in Table III were obtained solving the RPA coupled equations (determinant) associated with the  $^{10}\text{Be}(\text{gs})$  pair-removal mode, making use, as explained in Sect. b of App. A, of two pairing coupling constants, to properly deal with the difference in matrix elements (overlaps) between core-core, core-halo and halo-halo two-particle configurations. In other words with a “selfconsistent” treatment of the halo particle states ( $\varepsilon_k > \varepsilon_F$ ), in particular of the  $d_{5/2}(0)$  halo state. The absolute differential cross sections displayed in the figure were calculated making use of the optical parameters of refs. [37, 48].

The two-nucleon spectroscopic amplitudes associated with the reaction  $^{12}\text{Be}(p,t)^{10}\text{Be}(\text{gs})$  correspond to the numerical coefficients appearing in Eq. (12) below, and associated with the wavefunction describing the neutron component of the  $^{12}\text{Be}$  ground state (cf. ref. [9]):

$$|\widetilde{0}\rangle = |0\rangle + \alpha|(p_{1/2}, s_{1/2})_{1-} \otimes 1^-; 0\rangle + \beta|(s_{1/2}, d_{5/2})_{2+} \otimes 2^+; 0\rangle + \gamma|(p_{1/2}, d_{5/2})_{3-} \otimes 3^-; 0\rangle, \quad (10)$$

with

$$\alpha = 0.10, \quad \beta = 0.35, \quad \text{and} \quad \gamma = 0.33, \quad (11)$$

and

$$|0\rangle = 0.37|s_{1/2}^2(0)\rangle + 0.50|p_{1/2}^2(0)\rangle + 0.60|d_{5/2}^2(0)\rangle, \quad (12)$$

the states  $|1^- \rangle$ ,  $|2^+ \rangle$ ,  $|3^- \rangle$  being the corresponding lowest states of  $^{10}\text{Be}$ , calculated with the help of a multipole separable interaction in the RPA (see e.g. Table IV). It is of notice that a rather similar absolute differential cross section to the one displayed in Fig. 13 for the  $^{12}\text{Be}(p,t)^{10}\text{Be}(\text{gs})$  reaction is obtained making use of the spectroscopic amplitudes provided by the RPA wavefunction describing the  $^{10}\text{Be}$  pair addition mode (see Table III and App. A). This can be seen from the results displayed in Fig. 14.

To assess the correctness of the structure description of  $|^{12}\text{Be}(\text{gs})\rangle$  provided by the wavefunction (10-12) and of the second order DWBA-reaction mechanism (successive, simultaneous plus non-orthogonality) employed to calculate the absolute value of the  $^{12}\text{Be}(p,t)^{10}\text{Be}(\text{gs})$

differential cross section, we compare in Fig. 15 the predictions of the model for the reaction  $^{10}\text{Be}(p,t)^{12}\text{Be}(gs)$  at 17 MeV triton bombarding energy with the experimental data. Theory provides an overall account of observation within experimental errors.

It is of notice that the components proportional to  $\alpha, \beta$  and  $\gamma$  of the state (10) can lead, in a  $^{12}\text{Be}(p,t)$  reaction, to the direct excitation of the  $1^-, 2^+$  and  $3^-$  states of  $^{10}\text{Be}$ . Such results will add to the evidence obtained in the reaction  $^1\text{H} (^{11}\text{Li}(gs), ^9\text{Li}(1/2^-; 2.69 \text{ MeV}))^3\text{H}$  [34] of phonon mediated pairing [26]. The role of these components is assessed by the fact that (wrongly) normalizing the state (12) to 1, one obtains a value of  $\sigma = 4.5 \text{ mb}$  ( $4.4^\circ \leq \theta_{CM} \leq 57.4^\circ$ ), a factor 2 larger than the experimental value [48] (see Fig. 15).

Let us now return to Fig. 13.<sup>4</sup> The ratio of the integrated absolute cross section at  $E_{CM} = 7 \text{ MeV}$  in the range  $10^\circ \leq \theta_{CM} \leq 50^\circ$  appropriate for planned experimental studies making use of inverse kinematic techniques [46] is,

$$R = \frac{\sigma(^{12}\text{Be}(p,t)^{10}\text{Be}(pv; 6\text{MeV}))}{\sigma(^{12}\text{Be}(p,t)^{10}\text{Be}(gs))} = \frac{16.0\text{mb}}{6.9\text{mb}} \approx 2.3, \quad (13)$$

a result which testifies to the clear distinction between occupied and empty states taking place at  $N = 6$ , and thus of the *bona fide* nature of this magic number for halo, drip line nuclei. The ratio (13) reflects the fact that the pairing Zero Point Fluctuations (ZPF in gauge space) displayed by the  $|^{10}\text{Be}(gs)\rangle$  as embodied in the pair addition and pair removal modes, and quantified by the absolute values of the associated two-nucleon transfer cross sections, are of the same order of magnitude. This is an intrinsic property of the vibrational modes, in the same way in which e.g. the width (lifetime) of a nuclear state is an intrinsic (nuclear structure) property of such a state. An experiment displaying an energy resolution better than the intrinsic width of the states under study will provide structure information. Otherwise, eventually an upper limit. Within this scenario and in keeping with the fact that the successive transfer induced by the single-particle potential is the intrinsically (structure) dominant contribution to the absolute two-particle transfer cross

<sup>4</sup> In the harmonic approximation, and assuming simultaneous transfer, the cross section  $\sigma(r)$  associated with the pair removal mode of a closed shell system ( $A_0(p,t)(A_0-2)(gs)$ ) coincides by definition with that of the reaction  $(A_0+2)(p,t)A_0(pv)$  ( $\sigma(pv)$ ) exciting the two-phonon pairing vibrational mode starting from the ground state of the  $(A_0+2)$  system, this pair addition mode acting as spectator. However, taking properly into account the contribution of successive transfer,  $\sigma(r)$  and  $\sigma(pv)$  are expected to differ because of the difference in Q-values associated with the corresponding intermediate, virtual, one-particle transfer states. This is the reason why the cross section associated with the reaction  $^{10}\text{Be}(p,t)^8\text{Be}(gs)$  ( $\sigma(r)$ ) shown in Fig. 13, differs from that of  $^{12}\text{Be}(p,t)^{10}\text{Be}(pv; 6 \text{ MeV})$  ( $\sigma(pv)$ ) displayed in the lower part of Fig. 19 (aside from the fact that the energy of 6 MeV has been used instead of the harmonic value of 4.8 MeV). In spite of this fact, the two cross sections ( $\sigma = 16 \text{ mb}$  and  $\sigma = 17.4 \text{ mb}$  respectively) are rather similar, testifying to the validity of the pairing vibrational scheme.

section,  $Q$ -value (kinematic) effects can strongly distort the picture. In particular in the case in which single-particle transfer channels are closed at the studied bombarding energies.

Let us elaborate on these arguments in the case in which the reaction  $^{12}\text{Be}(p,t)^{10}\text{Be}$  populates the  $^{10}\text{Be}$  ground state, where the two correlated nucleons participating in the process are the two valence neutrons of  $^{12}\text{Be}(gs)$ . As the first neutron leaves  $^{12}\text{Be}(gs)$ , it leads to  $^{11}\text{Be}(j^\pi)$  where  $j^\pi$  labels  $2s_{1/2}$ ,  $1p_{1/2}$  and  $1d_{5/2}$ . In Fig. 16 we report, for concreteness, the  $Q$ -value scenario where  $j^\pi = 1/2^+$ , although the calculations of the absolute cross sections displayed in Figs. 13 and 14 were carried out making use of the full wavefunction, and thus of all possible ( $j^\pi = 1/2^+$ ,  $1/2^-$  and  $5/2^+$ ) intermediate states in the  $^{11}\text{Be}(j^\pi) + d$  channel. Of notice that, because of ground state correlations, situations in which  $j^\pi = 3/2^-(1p_{3/2}^{-1})$  and  $1/2^+(1s_{1/2}^{-1})$  are also possible (as hole states). The corresponding contributions are not negligible (see Table 3), although the most important ones arise from those mentioned above.

The case in which one populates the excited pairing vibrational state  $^{10}\text{Be}(pv; 6 \text{ MeV})$  is illustrated in Fig. 17. The fermions involved correspond to the correlated (valence) holes characterizing the ground state of  $^8\text{Be}$ , the two correlated (valence) neutrons building the  $^{12}\text{Be}$  ground state acting, in the harmonic approximation, only as spectators. Within this scenario, the most important contributions to the  $^{11}\text{Be}(j^\pi) + d$  intermediate states are hole states moving in the  $1p_{3/2}$  and  $1s_{1/2}$  orbitals. As seen from the figure, at  $E_{CM} = 5 \text{ MeV}$ , the  $^{11}\text{Be}(j^\pi)$  channels (e.g.  $^{11}\text{Be}(p_{3/2}^{-1}; 4\text{MeV})$ ) are barely open, thus quenching in a major way the excitation of the  $^{10}\text{Be}(pv; 6 \text{ MeV})$  state. The closing or opening of single-particle transfer channels due to  $Q$ -value effects, may constitute a unique opportunity to learn about the mechanism which is at the basis of two-nucleon transfer reaction processes (see Figs. 18-20). By properly adjusting the bombarding conditions (excitation function), one may tune on situations in which two-particle transfer switches from successive- to simultaneous-dominated transfer regimes.

Simple mechanical interpretations of the above mentioned  $Q$ -value effects can be given within the framework of the semiclassical approximation [17]. The transfer formfactors associated with the excitations of pairing correlated modes are, as a rule, smoothly varying functions along the trajectories of relative motion, displaying none or few nodes, in the neighborhood of the distance of closest approach. To obtain the variety of contributions to the two-nucleon transfer amplitudes the different formfactors are to be weighted with (imaginary) exponentials (i.e. periodic functions), resulting from the mismatch in mo-

momentum (recoil effects, Galilean-like transformations), and in stationary state phases (i.e.  $\exp\{-iEt/\hbar\}$ ) associated with the different relative orbitals. Large transfer amplitudes and eventually two-nucleon transfer cross sections are obtained when the arguments of the phases appearing in the imaginary exponential are small along the relative motion trajectory (little mismatch). The situation is reversed when the large (stationary) energy differences are not compensated by recoil effects and viceversa. In this case, the harmonic functions change rapidly sign along the relative motion trajectories, thus canceling the (smooth behavior) transfer formfactor contributions (large mismatch).

The extension (of the same arguments) to situations of long wavelength of relative motion (fully quantal scenario) can be made in terms of the WKB approximation (e.g. in terms of Stokes lines), as well as in terms of the Feynman path integral method. In this case all possible trajectories are to be considered. The associated formfactors are weighted with action phases. The different amplitudes thus result from the interweaving of these two types of functions. Depending on their mismatch different bombarding energies, angles, etc. will be privileged over others, as in the simpler (semiclassical) scenario discussed above.

## VI. CONCLUSIONS

It is an open question whether (mainly) phonon mediated neutron halo pairing can lead to a well developed (quasi harmonic) pairing vibrational multiphonon band. Inverse kinematics two-particle transfer processes, as well as standard two-particle transfer reactions can test the validity of the harmonic spectrum discussed above, and thus the actual nature of the  $N = 6$  shell closure, as well as shed light on the role medium polarization effects play in these fragile, highly polarizable systems. In particular concerning the induced pairing interaction. The question of how large the coupling between particle-hole phonons and the  $(n_a = 1, n_r = 1)$  pairing modes is, could also be tested through the above mentioned two-particle transfer experiments. Last, but not least, the NFT description of structure and reactions provides a natural framework for the calculation of the optical potential, a possibility which would bring one step further the concrete realization of the fact that structure and reactions are but two aspects of the same physics, in particular in the case of halo nuclei.

Discussions with I. Tanihata and R. Kanungo are gratefully acknowledged.

Financial support from the Ministry of Science and Innovation of Spain Grant No. FPA2009-07653 is acknowledged by G. P.

F.B. acknowledges financial support from the Ministry of Science and Innovation of Spain grants FPA2009-07653 and ACI2009-1056.

- 
- [1] D. Brink and R. A. Broglia. *Nuclear Superfluidity, 2nd. ed.* Cambridge University Press, Cambridge, 2010.
  - [2] P. W. Anderson. Random-Phase Approximation in the theory of superconductivity. *Phys. Rev.*, 112:1900, 1958.
  - [3] P. Wölfle. volume VII-A of *Progress in Low Temperature Physics*, page 191. Ed. D.F. Brewer, 1978.
  - [4] R. A. Broglia, O. Hansen, and C. Riedel. Two-neutron transfer reactions and the pairing model. *Adv. Nucl. Phys.*, 6:287, 1973.
  - [5] F. Barranco, R. A. Broglia, G. Gori, E. Viguzzi, P. F. Bortignon, and J. Terasaki. Surface vibrations and the pairing interaction in nuclei. *Phys. Rev. Lett.*, 83:2147, 1999.
  - [6] E. R. Flynn, G. J. Igo, and R. A. Broglia. Three-phonon monopole and quadrupole pairing vibrational states in  $^{206}\text{Pb}$ . *Phys. Lett. B*, 41:397, 1972.
  - [7] P.F. Bortignon, R.A. Broglia, and D.R. Bes. On the convergence of the nuclear field theory perturbation expansion for strongly anharmonic systems. *Phys. Lett. B*, 76:153, 1978.
  - [8] F. Barranco, P. F. Bortignon, R. A. Broglia, G. Colò, and E. Viguzzi. The halo of the exotic nucleus  $^{11}\text{Li}$ : a single Cooper pair. *Europ. Phys. J. A*, 11:385, 2001.
  - [9] G. Gori, F. Barranco, E. Viguzzi, and R. A. Broglia. Parity inversion and breakdown of shell closure in be isotopes. *Phys. Rev. C*, 69:041302, 2004.
  - [10] D. R. Bès, R. A. Broglia, G. G. Dussel, R. J. Liotta, and H. M. Sofía. The nuclear field treatment of some exactly soluble models. *Nucl. Phys. A*, 260:1, 1976.
  - [11] D. R. Bès, R. A. Broglia, G. G. Dussel, R. J. Liotta, and H. M. Sofia. Application of the nuclear field theory to monopole interactions which include all the vertices of a general force. *Nucl. Phys. A*, 260:27, 1976.
  - [12] D. R. Bès, R. A. Broglia, G. G. Dussel, R. J. Liotta, and R. P. J. Perazzo. On the many-body foundation of the Nuclear Field Theory. *Nucl. Phys. A*, 260:77, 1976.

- [13] D.R. Bès and R. A. Broglia. Equivalence between Feynman–Goldstone and particle–phonon diagrams for finite many body systems. In G. Alaga, V. Paar, and L. Sips, editors, *Problems of Vibrational Nuclei, in Procs. of the topical Conference on Problems of Vibrational Nuclei*, page 1, Amsterdam, 1975. North Holland.
- [14] B.R. Mottelson. Elementary modes of excitation in the nucleus (Nobel lecture). *Rev. Mod. Phys.*, 48:375, 1976.
- [15] P. F. Bortignon, R. A. Broglia, D. R. Bès, and R. Liotta. Nuclear field theory. *Phys. Rep.*, 30:305, 1977.
- [16] R. A. Broglia, B. R. Mottelson, D. R. Bès, R. Liotta, and H. M. Sofía. Treatment of the spurious state in Nuclear Field Theory. *Physics Letters B*, 64:29, 1976.
- [17] R. A. Broglia and A. Winther. *Heavy Ion Reactions, 2nd ed.* Westview Press, Perseus Books, Boulder, 2005.
- [18] D. R. Bès and R. A. Broglia. Pairing vibrations. *Nucl. Phys.*, 80:289, 1966.
- [19] L. N. Cooper. Bound electron pairs in a degenerate Fermi gas. *Phys. Rev.*, 104:1189, 1956.
- [20] A. J. Leggett. *Quantum Liquids*. Oxford University Press, Oxford, 2006.
- [21] B. D. Josephson. Possible new effects in superconductive tunnelling. *Phys. Lett.*, 1:251, 1962.
- [22] M. H. Cohen, L. M. Falicov, and J. C. Phillips. Superconductive tunneling. *Phys. Rev. Lett.*, 8:316, 1962.
- [23] G. Potel, A. Idini, F. Barranco, E. Vigezzi, and R. A. Broglia. Single Cooper pair transfer in stable and in exotic nuclei. *arXiv:0906.4298v1 [nucl-th]*.
- [24] R.P. Feynman. *Quantum Electrodynamics*. Advance Book Program, Benjamin, Reading, Mass., 1961.
- [25] A. Bohr and B. R. Mottelson. *Nuclear Structure, Vol.II*. Benjamin, New York, 1975.
- [26] G. Potel, F. Barranco, E. Vigezzi, and R. A. Broglia. Evidence for phonon mediated pairing interaction in the halo of the nucleus  $^{11}\text{Li}$ . *Phys. Rev. Lett.*, 105:172502, 2010.
- [27] G. Potel, F. Barranco, F. Marini, A. Idini, E. Vigezzi, and R. A. Broglia. Calculation of the transition from pairing vibrational to pairing rotational regimes between magic nuclei  $^{100}\text{Sn}$  and  $^{132}\text{Sn}$  via two-nucleon transfer reactions. *Phys. Rev. Lett.*, 107:092501, 2011.
- [28] G. Potel and R.A Broglia. Pairing correlations with single Cooper pair transfer to individual quantal states. In R.A. Broglia and V. Zelevinsky, editors, *50 Years of Nuclear BCS*, Singapore. World Scientific, (in press).



- [29] G. Potel, A. Idini, F. Barranco, E. Vigezzi, and R. A. Broglia. Quantitative study of coherent pairing modes with two neutron transfer: Sn-isotopes. *ArXiv:1210.5085v.1 [nucl-th]*, 2012.
- [30] J. Bardeen, L. N. Cooper, and J. R. Schrieffer. Microscopic theory of superconductivity. *Phys. Rev.*, 106:162, 1957.
- [31] A. Bohr and B. R. Mottelson. *Nuclear Structure, Vol.I*. Benjamin, New York, 1969.
- [32] C. Bachelet, G. Audi, C. Gaulard, C. Guénaut, F. Herfurth, D. Lunney, M. de Saint Simon, and C. Thibault. New Binding Energy for the Two-Neutron Halo of  $^{11}\text{Li}$ . *Phys. Rev. Lett.*, 100:182501, 2008.
- [33] M. Smith, M. Brodeur, T. Brunner, S. Ettenauer, A. Lapierre, R. Ringle, V. L. Ryjkov, F. Ames, P. Bricault, G. W. F. Drake, P. Delheij, D. Lunney, F. Sarazin, and J. Dilling. First Penning-trap mass measurement of the exotic halo nucleus  $^{11}\text{Li}$ . *Phys. Rev. Lett.*, 101:202501, 2008.
- [34] I. Tanihata, M. Alcorta, D. Bandyopadhyay, R. Bieri, L. Buchmann, B. Davids, N. Galinski, D. Howell, W. Mills, S. Mythili, R. Openshaw, E. Padilla-Rodal, G. Ruprecht, G. Sheffer, A. C. Shotter, M. Trinczek, P. Walden, H. Savajols, T. Roger, M. Caamano, W. Mittig, P. Roussel-Chomaz, R. Kanungo, A. Gallant, M. Notani, G. Savard, and I. J. Thompson. Measurement of the two-halo neutron transfer reaction  $^1\text{H}(^{11}\text{Li}, ^9\text{Li})^3\text{H}$  at 3A MeV. *Phys. Rev. Lett.*, 100:192502, 2008.
- [35] P. G. Young and R. H. Stokes. New states in  $^9\text{Li}$  from the reaction  $^7\text{Li}(t, p)^9\text{Li}$ . *Phys. Rev. C*, 4:1597, 1971.
- [36] F. Ajzenberg-Selove, E. R. Flynn, and O. Hansen.  $(t, p)$  reactions on  $^4\text{He}$ ,  $^6\text{Li}$ ,  $^7\text{Li}$ ,  $^9\text{Be}$ ,  $^{10}\text{B}$ ,  $^{11}\text{B}$ , and  $^{12}\text{C}$ . *Phys. Rev. C*, 17, 1978.
- [37] H. An and C. Cai. Global deuteron optical model potential for the energy range up to 183 MeV. *Phys. Rev. C*, 73:054605, 2006.
- [38] C. Mahaux, P. F. Bortignon, R. A. Broglia, and C. H. Dasso. Dynamics of the shell model. *Phys. Rep.*, 120:1, 1985.
- [39] R. A. Broglia, V. Paar, and D. R. Bes. Diagrammatic perturbation treatment of the effective interaction between two-photon states in closed shell nuclei: The  $J^\pi = 0^+$  states in  $^{208}\text{Pb}$ . *Phys. Lett. B*, 37(2):159, 1971.
- [40] J.P. Fernandez-Garcia, M.A.G. Alvarez, A.M. Moro, and M. Rodriguez-Gallardo. Simultaneous analysis of elastic scattering and transfer/breakup channels for the  $^6\text{He}+^{208}\text{Pb}$  reaction

- at energies near the Coulomb barrier. *Phys. Lett. B*, 693(3):310, 2010.
- [41] J.P. Fernandez-Garcia, M. Rodriguez-Gallardo, M.A.G. Alvarez, and A.M. Moro. Long range effects on the optical model of  ${}^6\text{He}$  around the Coulomb barrier. *Nucl. Phys. A*, 840(1-4):19, 2010.
  - [42] R.A. Broglia, G. Pollaro, and A. Winther. On the absorptive potential in heavy ion scattering. *Nuclear Physics A*, 361:307, 1981.
  - [43] G. Pollaro, R.A. Broglia, and A. Winther. Calculation of the imaginary part of the heavy ion potential. *Nuclear Physics A*, 406:369, 1983.
  - [44] W. Dickhoff and D. Van Neck. *Many-Body Theory Exposed!: Propagator Description of Quantum Mechanics in Many-Body Systems*. World Scientific, 2005.
  - [45] B. Jennings. Non-observability of spectroscopic factors. *arXiv:1102.3721*, 2011.
  - [46] R. Kanungo et. al. Study of nuclear pairing through  ${}^{12}\text{Be}(p,t)$  reaction. TRIUMF approved proposal number S1338, 2012.
  - [47] D. E. Alburger, E. K. Warburton, A. Gallmann, and D. H. Wilkinson. Decay of the 6.18-MeV  $J^\pi = 0^+$  level of  ${}^{10}\text{Be}$ . *Phys. Rev.*, 185:1242, 1969.
  - [48] H. T. Fortune, G.-B. Liu, and D. E. Alburger.  $(sd)^2$  states in  ${}^{12}\text{Be}$ . *Phys. Rev. C*, 50:1355, 1994.
  - [49] R. A. Broglia, C. Riedel, and T. Udagawa. Coherence properties of two-neutron transfer reactions and their relation to inelastic scattering. *Nucl. Phys. A*, 169:225, 1971.
  - [50] R. A. Broglia, C. Riedel, and T. Udagawa. Sum rules and two-particle units in the analysis of two-neutron transfer reactions. *Nucl. Phys. A*, 184:23, 1972.
  - [51] B. R. Mottelson. Selected topics in the theory of collective phenomena in nuclei. In G. Racah, editor, *International School of Physics “Enrico Fermi” Course XV , Nuclear Spectroscopy*, page 44, New York, 1962. Academic Press.
  - [52] D. R. Bès and R. A. Sorensen. The pairing-plus-quadrupole model. *Adv. Nucl. Phys.*, 2:129, 1969.
  - [53] B. F. Bayman. *Seniority, Quasiparticles and Collective Vibrations*. Unpublished, 1960. Lecture notes at the Palmer Physical Laboratory, Princeton University.
  - [54] D. R. Bès and R. A. Broglia. Effect of the multipole pairing and particle-hole fields in the particle-vibration coupling of  ${}^{209}\text{Pb}$ . I. *Phys. Rev. C*, 3:2349, 1971.
  - [55] D. R. Bès and R. A. Broglia. Effect of the multipole pairing and particle-hole fields in the

- particle-vibration coupling of  $^{209}\text{Pb}$ . II. *Phys. Rev. C*, 3:2371, 1971.
- [56] D. R. Bès and R. A. Broglia. Effective operators and the analysis of single-neutron transfer reactions on closed-shell nuclei. *Phys. Rev. C*, 3:2389, 1971.
  - [57] M.G. Mayer and J.H.D. Jensen. *Elementary Theory of Nuclear Shell Structure*. Wiley & Sons, New York, NY, 1955.
  - [58] A. Bohr. Rotational motion in nuclei (Nobel lecture). *Rev. Mod. Phys.*, 48:365, 1976.
  - [59] H. Esbensen and G. F. Bertsch. Nuclear surface fluctuations: Charge density. *Phys. Rev. C*, 28:355, 1983.
  - [60] F. Barranco and R. A. Broglia. Effect of surface fluctuations on the nuclear density. *Phys. Rev. Lett.*, 59:2724, 1987.
  - [61] S.G. Nilsson. Binding states of individual nucleons in strongly deformed nuclei. *Dan. Fys. Medd.*, 29:16, 1955.
  - [62] G.C. Ball, L. Buchmann, B. Davids, R. Kanungo, C. Ruiz, and C.E. Svensson. Physics with reaccelerated radioactive beams at TRIUMF-ISAC. *J. Phys. G*, 38:024003, 2011.
  - [63] N. Bohr. Neutron capture and nuclear constitution. *Nature*, 137:344, 1936.
  - [64] D. Bès and J. Kurchan. *The treatment of Collective Coordinates in Many-Body Systems*. World Scientific, Singapore, 1990.
  - [65] John Bardeen and David Pines. Electron-phonon interaction in metals. *Phys. Rev.*, 99:1140, 1955.
  - [66] Pickett W.E. Electron and phonons in  $c_{60}$ -based materials. In H. Ehrenreich and F. Spaepen, editors, *Solid State Physics : Fullerenes*, San Diego, 1994. Academic Press.
  - [67] Lieber C.M. and Zhang Z. Physical properties of metal-doped fullerene superconductors. In H. Ehrenreich and F. Spaepen, editors, *Solid State Physics : Fullerenes*, San Diego, 1994. Academic Press.
  - [68] O. Gunnarsson. *Alkali-doped Fullerenes: Narrow-band Solids with Unusual Properties*. World Scientific, Singapore, 2004.
  - [69] C.C. Chancey and O'Brien M.C.M. *The Jahn-Teller effect in  $C_{60}$  and other icosahedral complexes*. Princeton University Press, Princeton, New Jersey, 1997.
  - [70] Dresselhaus G. Dresselhaus M.S. and Eklund P.C. *Science of Fullerenes and Carbon Nanotubes*. Princeton University Press, Princeton, New Jersey, 1997.
  - [71] R. A. Broglia, G. Coló, G. Onida, and H. E. Roman. *Solid State Physics of Finite Systems:*

*metal clusters, fullerenes, atomic wires*. Springer Verlag, Berlin, Heidelberg, 2004.

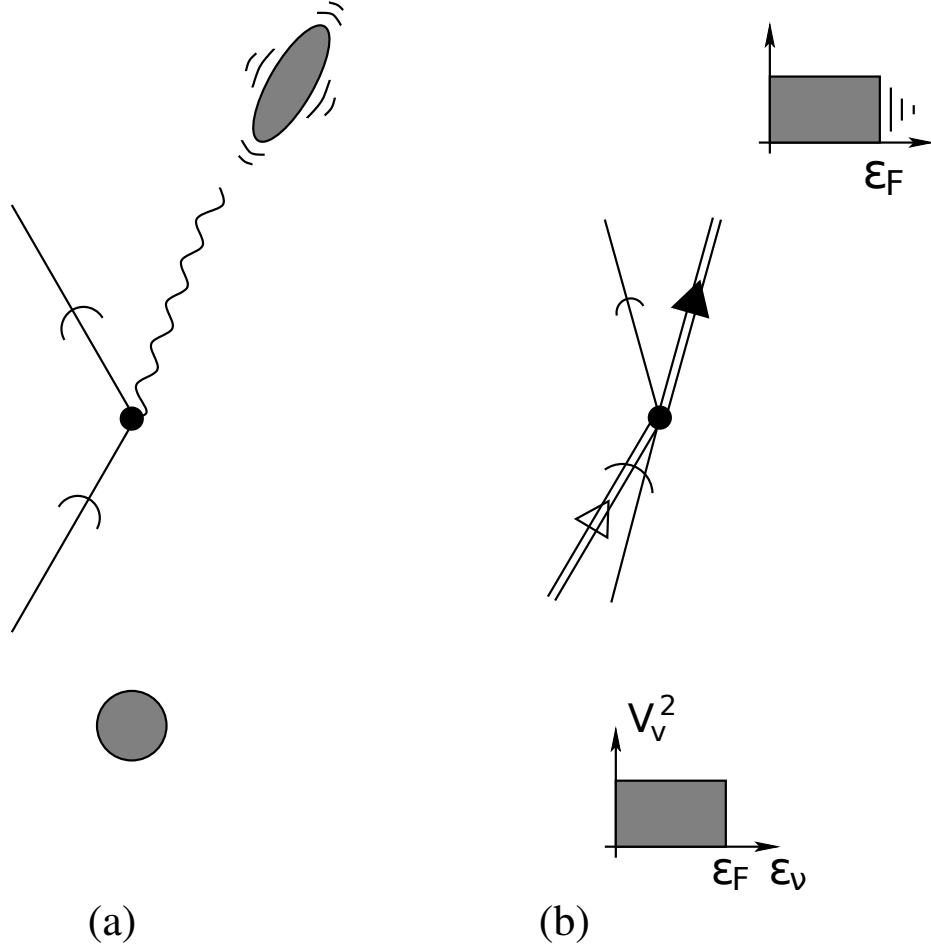


Figure 1. Diagrammatic representation of: a) inelastic scattering process (transfer quantum number  $\beta = 0$ ) of a collective particle-hole like (quadrupole surface vibration) induced by the nonhomogeneous time dependent field created by a nucleon (projectile, curved arrowed line) passing by the target nucleus, b) two-particle transfer process in which a dineutron is stripped from the incoming triton exciting the pair addition mode (transfer quantum number  $\beta = +2$ ) of e.g. a closed shell system (double lines labeled with a conventionally empty arrow corresponds to two neutrons bound in the projectile (triton); when labeled by a solid arrow, it corresponds to a pair addition mode, i.e. to two nucleons bound to the core nucleus). The solid dot indicates the particle vibration coupling vertex measured by the strength  $\Lambda_\alpha(\beta)$ , where the subindex  $\alpha$  indicate the angular momentum and eventually, if the mode is fragmented, whether the state is the lowest, next to lowest, etc. in energy.

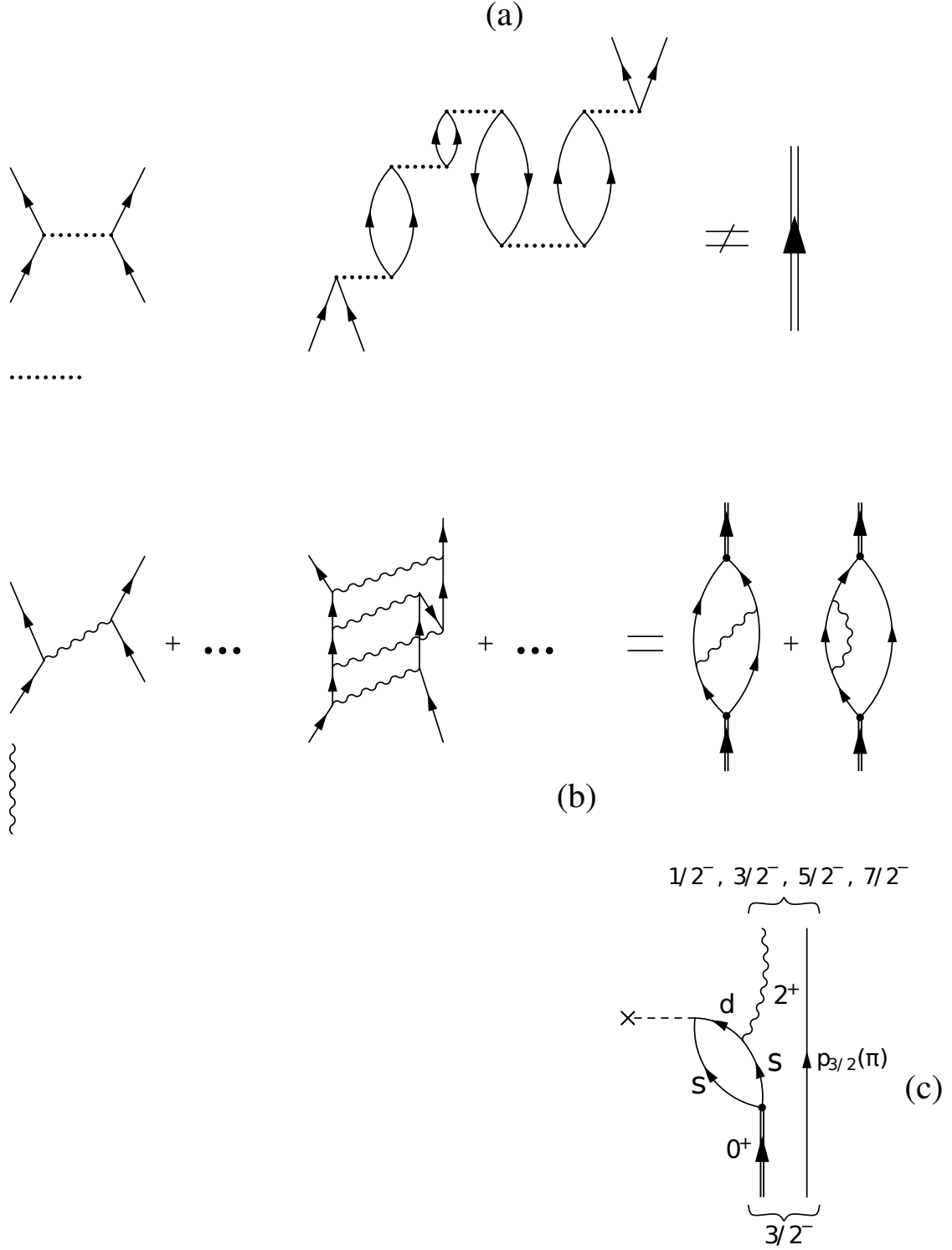


Figure 2. In the case of  $^{11}\text{Li}$  the bare interaction (e.g. Argonne  $v_{14}$   $N-N$  potential; horizontal dotted line) acting to infinite order between the halo neutrons (see (a)) does not lead to a bound Cooper pair (double solid arrowed line), but merely shifts downwards (lowers the energy) of the resonant configurations  $s_{1/2}^2(0)$  and  $p_{1/2}^2(0)$  by about 100 keV individually, without leading to any appreciable mixing [8]. The exchange of a dipole pigmy resonance of the halo field and of a quadrupole vibration of the  $^9\text{Li}$  core (wavy lines, see (b)) provides essentially all of the glue for the Cooper pair to become bound ( $S_{2n} = 330$  keV, theory [8] as compared to the experimental data of  $378 \pm 5$  keV [32];  $369.15 \pm 0.65$  keV [33]). In (c) a schematic representation of the  $^{11}\text{Li}(p, t)^9\text{Li}(1/2^-)$  process (see [26, 34]) is displayed (see also Figs. 3 and 4).

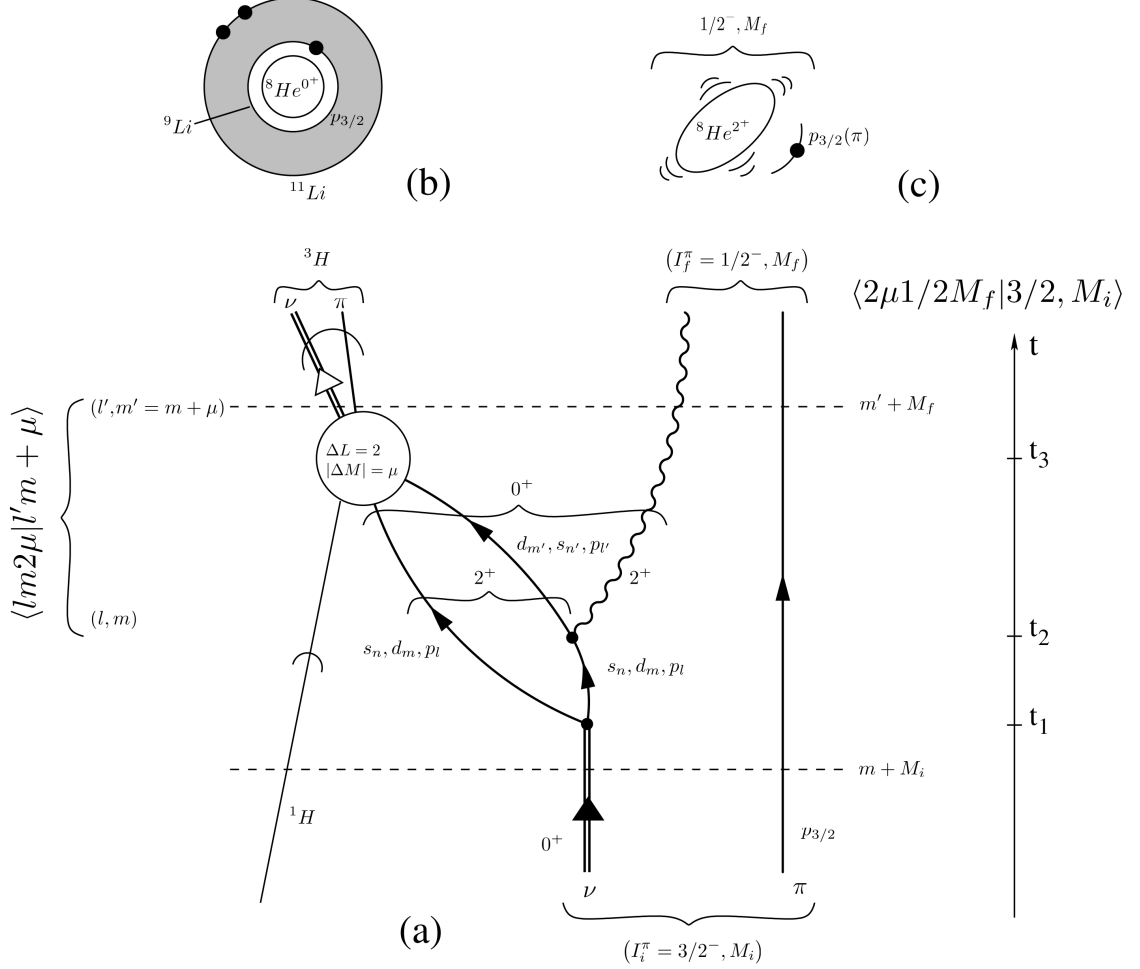


Figure 3. (a) NFT-Feynman diagram associated with the process  $^1\text{H}(^{11}\text{Li}(\text{gs}), ^9\text{Li}(1/2^-; 2.69 \text{ MeV})^3\text{H})$ , which treats on equal footing the nuclear structure ( $\uparrow\uparrow^{2+}, \uparrow\uparrow^{2+}, \uparrow$ ) and the reaction mechanism ( $\uparrow, \uparrow\uparrow$ ). The neutron correlated Cooper pair (pair addition mode), has a somewhat different structure when bound to  $^9\text{Li}$  to make  $^{11}\text{Li}$ , than to the proton to make the triton ( $^3\text{H}$ ) (depicted with a solid and with an open arrow respectively). This is the reason why there is a finite overlap, called  $\Omega_n (n = 0, 1, \dots)$  between the corresponding relative motion wavefunctions displaying zero, one, etc. nodes (cf. e.g. [4] and references therein). In keeping with this fact one can posit that although  $(p, t)$  reactions are quite specific to probe pairing correlations in nuclei, in particular in the case of the  $^{11}\text{Li}$  neutron Cooper pair, they display limitations. In particular the specific probe in the case under discussion is the  $^{11}\text{Li}(^9\text{Li}, ^{11}\text{Li})^9\text{Li}$  reaction ( $\Omega_n = \delta(n, 0)$ ), although obviously much more demanding experimentally. Curly brackets indicate angular momentum coupling, while horizontal dashed lines indicate magnetic quantum number conservation. In (b) and (c) a schematic representation of the initial ( $^{11}\text{Li}$ ) and final ( $^9\text{Li}(1/2^-, M_f; 2.69 \text{ MeV})$ ) nuclear states are given, respectively. The ordinate to the right indicates time. Following NFT of both structure [10–16] and reaction [17] processes, all possible time orderings are to be considered in the calculations. It is of notice that curved arrowed lines indicate continuum scattering states, while standard arrowed lines correspond to bound states.

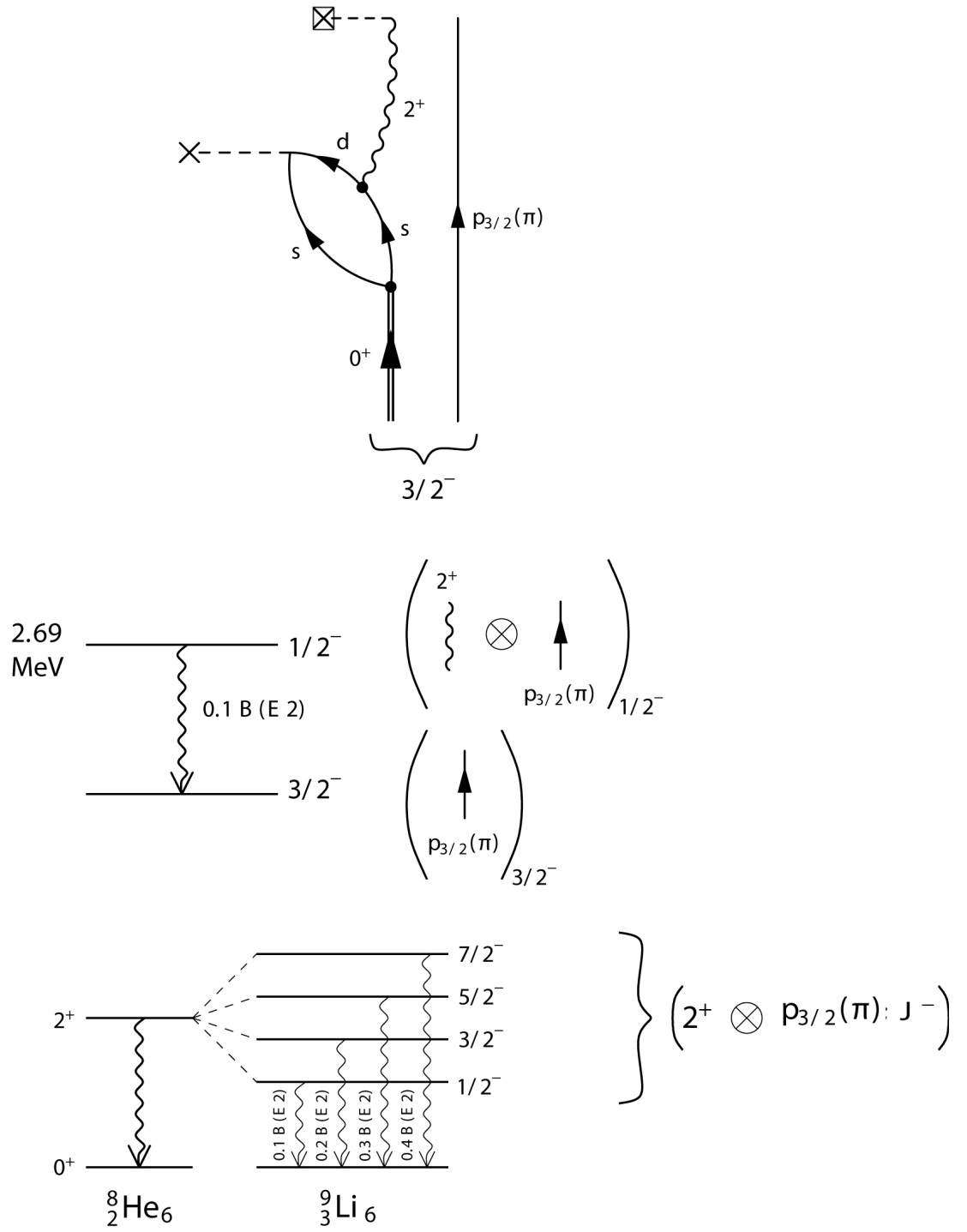


Figure 4. *Gedanken* (two-particle transfer)-( $\gamma$  decay) coincidence experiments aimed at better individuating the couplings involved in the neutron halo Cooper pair correlations in  $^{11}\text{Li}$  and of the  $1/2^-$  member of  $^9\text{Li}$  excited in the  $^1\text{H}(^{11}\text{Li}, ^9\text{Li})^3\text{H}$  reaction [26, 34].



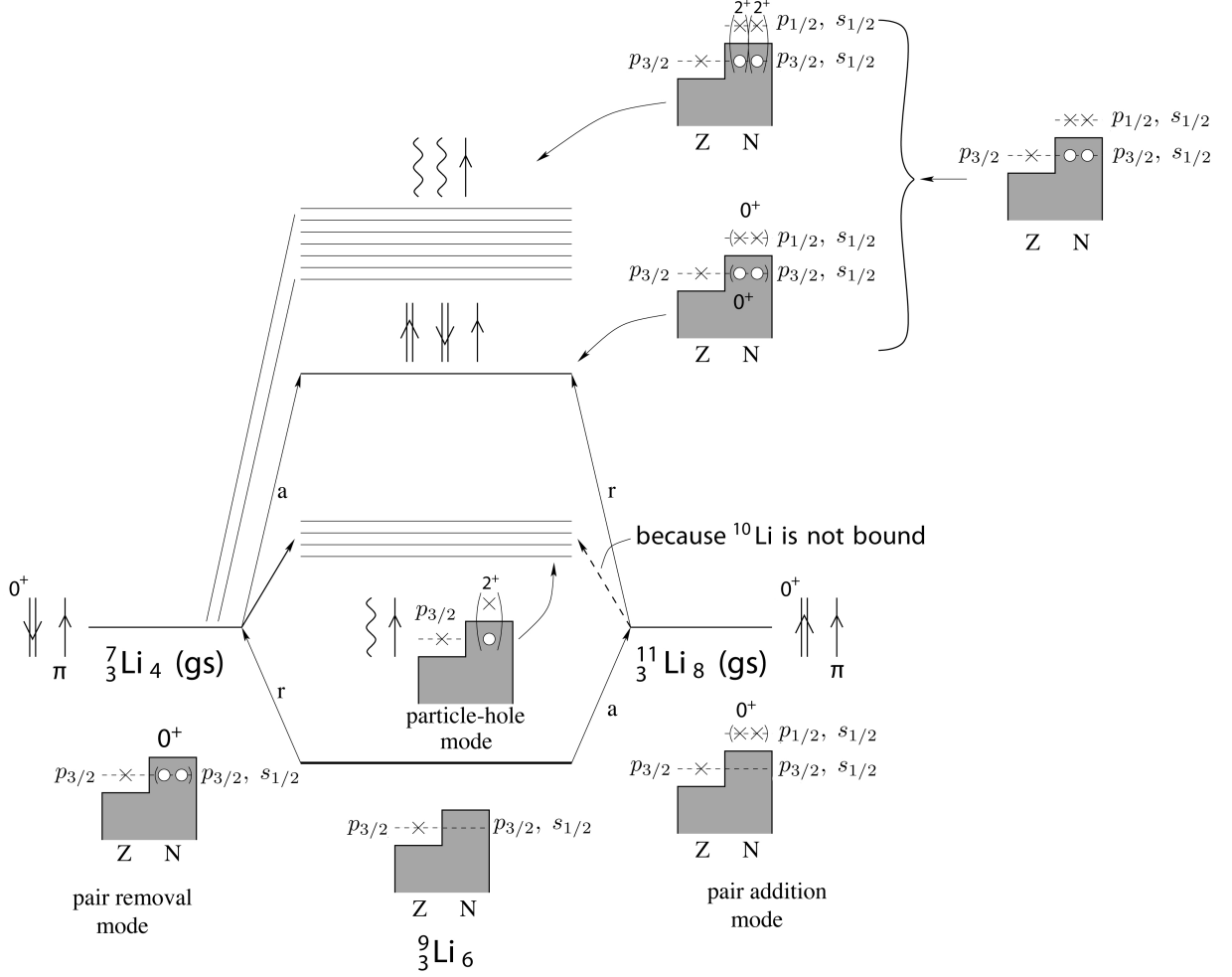


Figure 5. Schematic representation of the phonon pairing ( $\beta = \pm 2$ ) and density vibrational ( $\beta = 0$ ) spectrum based on  ${}^9_3\text{Li}_6$  (harmonic approximation), constructed making an analogy with studies of two-particle transfer reactions carried out around  ${}^{208}\text{Pb}$  (cf. e.g. [1] p. 109 Fig. 5.5 and refs. therein; see also [8]). The Fermi representation of occupied proton ( $Z$ ) and neutron ( $N$ ) states is schematically shown in terms of grey areas, where holes are shown as empty circles, and particles are indicated in terms of crosses. A single-headed line pointing upwards (downwards) represent a particle (hole) neutron or proton state. A double arrow indicates the correlated neutron pair addition (subtraction) modes. The predicted two-particle transfer cross sections  $a, r$  and excitation energy  $E_{pv}$  associated with the two-phonon (pair-addition), (pair-subtraction) and ( $2p-2h$  like excitation) pairing vibrational (pv) state expected in  ${}^9\text{Li}$  are, in the harmonic approximation:  $E_{pv} = 5.7$  MeV,  $a = d\sigma({}^{11}\text{Li}(p, t) {}^9\text{Li}(gs); \theta = 60^\circ) / d\Omega = 0.7$  mb/sr [34], and  $r = d\sigma({}^7\text{Li}(t, p) {}^9\text{Li}(gs); \theta = 60^\circ) / d\Omega = 3.0$  mb/sr [35], (see also Fig. 6).

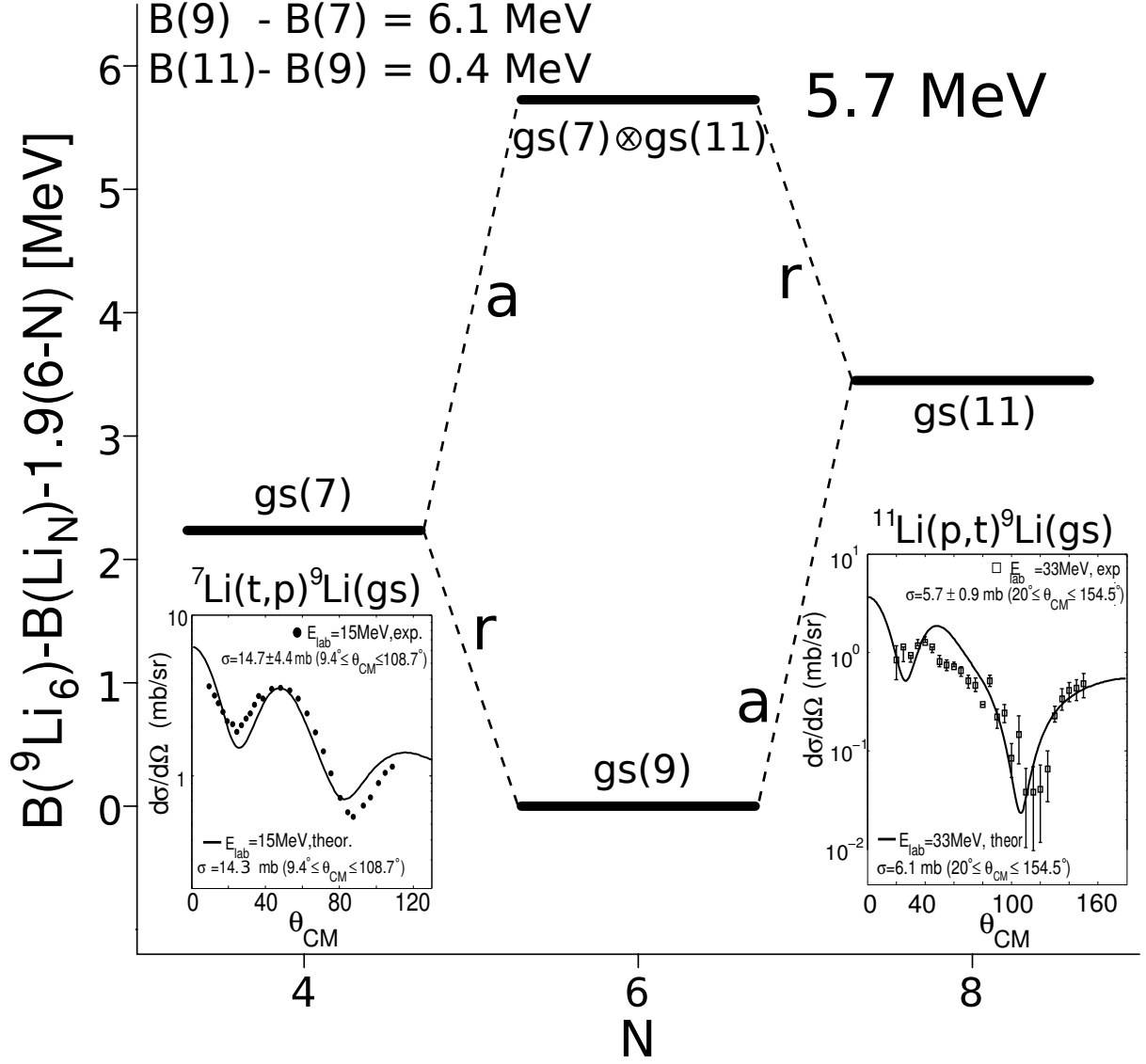


Figure 6. Pairing vibrations around  $^9\text{Li}$  and absolute cross sections associated with removal [35] (see also [36]) and addition [34] modes. The theoretical **absolute** differential cross sections for  $^{11}\text{Li}(p,t)^9\text{Li}(gs)$  (addition: a) is reported in [26]. The theoretical **absolute** differential cross section associated with the reaction  $^7\text{Li}(t,p)^9\text{Li}(gs)$  (removal: r) was carried out making use of the wavefunction associated with the RPA solution of the pairing Hamiltonian (see [4], [18] and App. A as well as Table 1), adjusting the coupling constant  $G$  to reproduce the correlation energy of the two neutron holes in the core of  $^9\text{Li}$  (i.e. in the ground state of  $^7\text{Li}$ ). The optical potential parameters used were taken from ref. [35, 37]. Of notice that throughout in this paper, in particular in connection with this figure, we report **absolute** differential cross sections (see also Table 2).

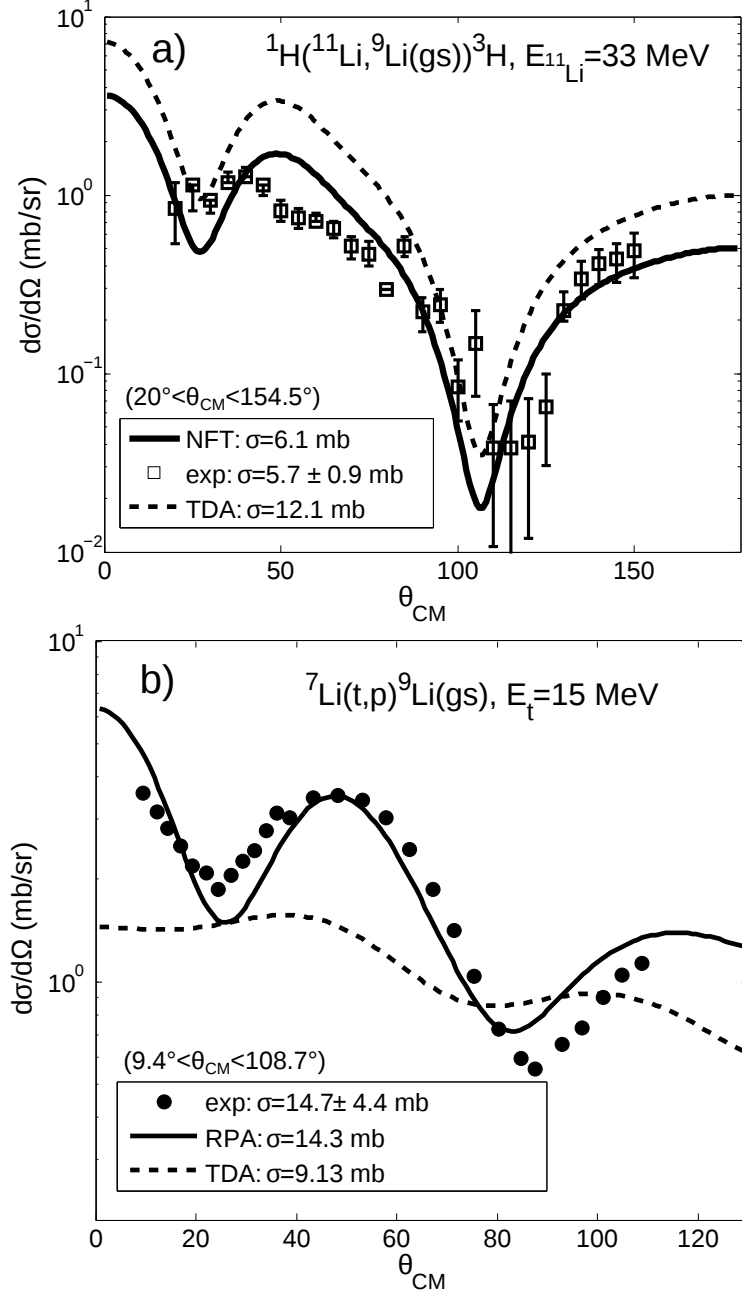


Figure 7. Absolute differential cross section of the pair addition and pair removal modes of  $^9\text{Li}$  in comparison with the experimental findings. (a) The NFT results of the calculations of the absolute values of  $d\sigma/d\Omega$  associated with the reaction  $^{11}\text{Li}(p, t) ^9\text{Li}(\text{gs})$  (pair addition mode) reported in Fig. 6 are compared with those labeled Tamm-Dancoff approximation (TDA), in which the interweaving of single-particle and particle-hole like vibrational modes are neglected while the  $|s^2\rangle$ ,  $|p^2\rangle$ ,  $|d^2\rangle$  components of the two-neutron wavefunction are normalized to one (see text). (b) The absolute value of the differential cross section  $d\sigma/d\Omega$  associated with the reaction  $^7\text{Li}(t, p) ^9\text{Li}(\text{gs})$  (pair removal mode) and calculated making use of the RPA two-nucleon transfer spectroscopic amplitudes ( $X^r, Y^r$ -values, Table 1) also reported in Fig. 6, is compared with that obtained neglecting ground state correlations and labeled TDA (see text).

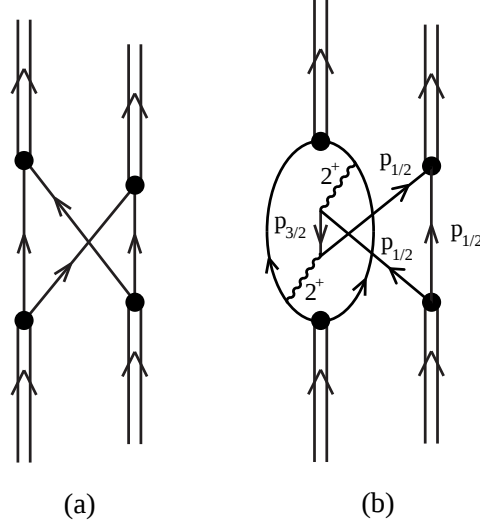


Figure 8. Pairing modes phonon-phonon interaction arising from: (a) Pauli principle processes between pairing modes, and (b) between single-particle and phonon-mediated induced pairing interaction (so called CO diagrams, cf. e.g. [38]. See also Fig. 10 (inset)).

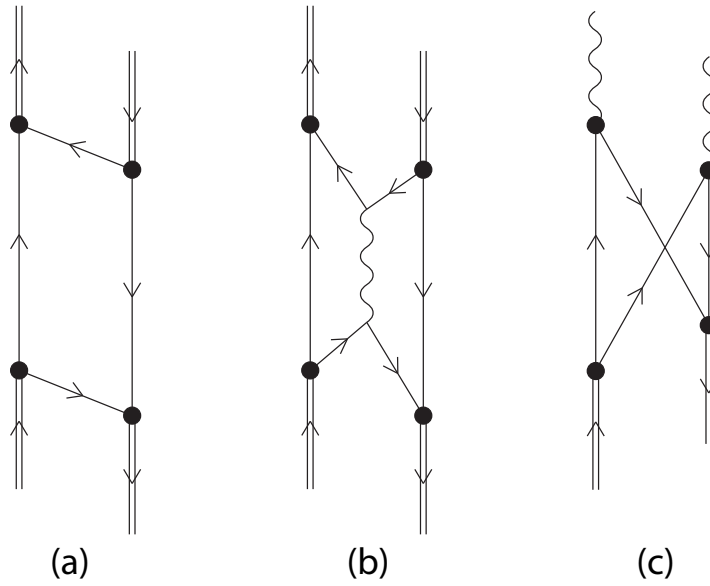


Figure 9. (a),(b) Examples of pair addition and pair removal modes interactions. (c) Interaction between the two-phonon pairing vibration state and the two-phonon particle-hole state.

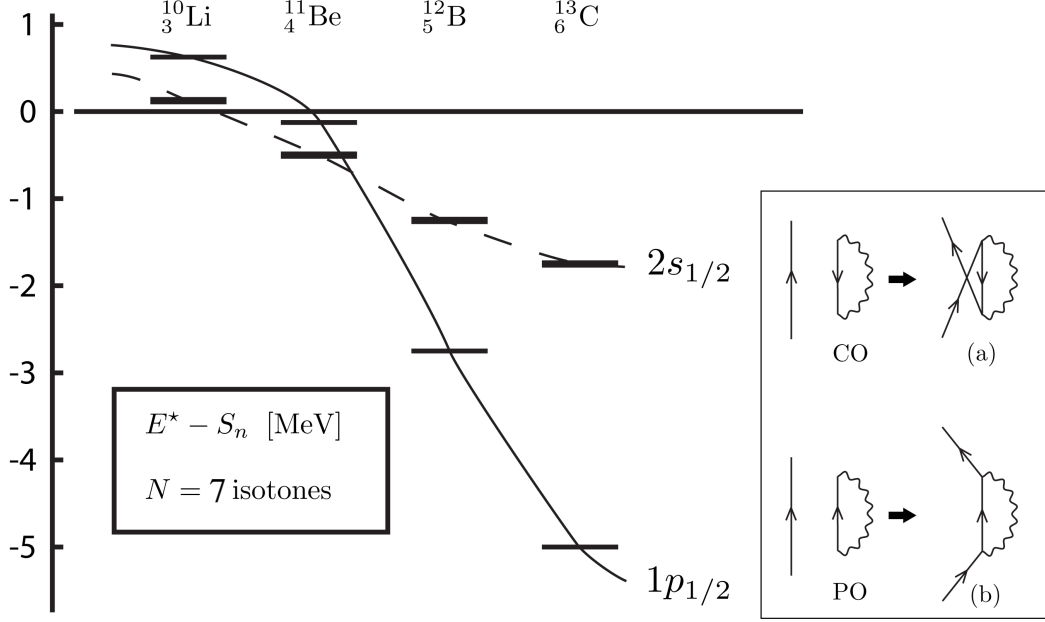


Figure 10. Single-particle states for  $N = 7$  isotones around  $^{11}\text{Be}$  associated with parity inversion. The thin horizontal lines represent the  $1p_{1/2}$  single-particle state, while the thick ones the  $2s_{1/2}$  orbital. In the case of  $^{10}\text{Li}$  one reports the centroid of the virtual and of the resonant states.  $E^*$  stands for excitation energy and  $S_n$  is the neutron separation energy. In the case of  $^{10}\text{Li}$  e.g.  $S_n = 0$ , while  $E^*_{s_{1/2}} = 0.2$  MeV and  $E^*_{p_{1/2}} = 0.5$  MeV. In the inset the correlation (CO) and polarization (PO) (virtual) contribution to the single-particle self energy are shown. An arrowed line pointing upwards represent a particle moving in a level with energy  $\varepsilon_k > \varepsilon_F$ , a downwards pointing line represent a hole state  $\varepsilon_i < \varepsilon_F$ , while a wavy line stands for a ph-like vibrational state. Their contribution to the real (single-particle “legs” propagating to  $\pm\infty$  times) processes dressing the  $1p_{1/2}$  and  $2s_{1/2}$  neutron states of  $^{10}\text{Li}$  and  $^{11}\text{Be}$  are (a) and (b) respectively. In the first case the phonon corresponds essentially only to the  $2^+$  vibration of the corresponding core ( $^9\text{Li}$  and  $^{10}\text{Be}$  respectively), and pushes the orbital upwards (Pauli principle, Lamb-shift-like process) making the dressed  $p_{1/2}$  orbital more strongly unbound than what it was originally in the Saxon–Woods potential (see [31] Eqs. (2-180)–(2-182) pp. 238 and 239). In the case of the  $2s_{1/2}$  orbital, it is mainly the process (b) which dresses the state making it almost bound (virtual state) as compared with the Saxon–Woods state. Within this context, it is of notice that in the binding of the two halo neutrons of  $^{11}\text{Li}$  to the  $^9\text{Li}$  core, it is essentially the pigmy resonance of  $^{11}\text{Li}$  which provides the largest contribution, the coupling to the  $2^+$  vibration of the core  $^9\text{Li}$  giving a small shift in energy (nonetheless, it is this weak component of the self energy which is responsible for the excitation, in the  $^{11}\text{Li}(p,t)^9\text{Li}$  reaction [34], of the  $1/2^-$ , 2.69 MeV state [26]). In the case of  $^{11}\text{Be}$  the (p-h) vibrations are the  $2^+$ ,  $1^-$  and  $3^-$  of the core  $^{10}\text{Be}$ , in keeping also with the fact that  $^{12}\text{Be}$  does not display a pigmy  $1^-$  resonance, not at least based on the ground state. It is of notice that graphs (a) and (b) give rise to an effective mass known as the  $\omega$ -mass. Associated with it are the  $Z(\omega) = (m_\omega/m)^{-1}$  occupation factors (discontinuity at the Fermi energy; for details see ref. [38] and refs. therein).

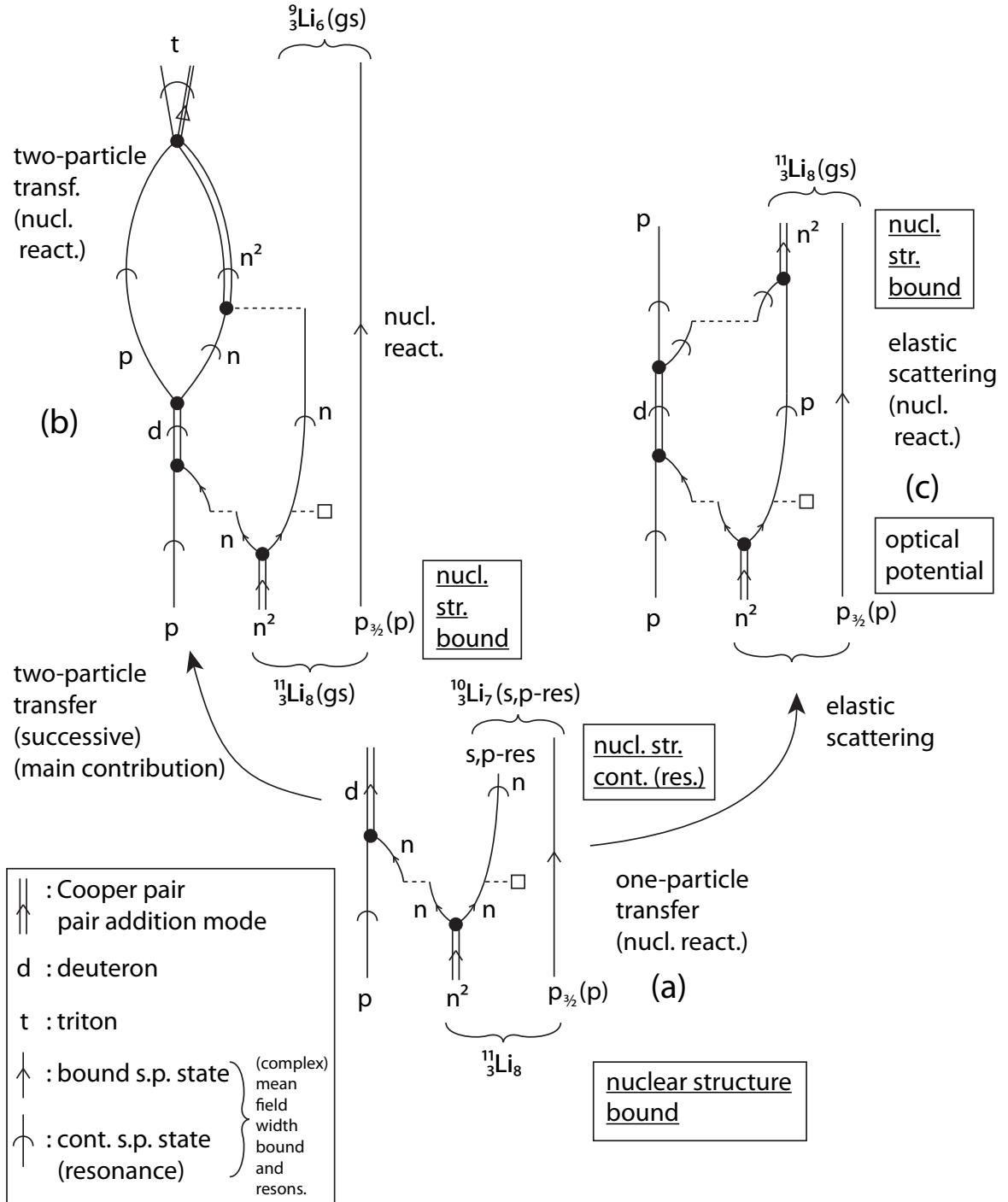
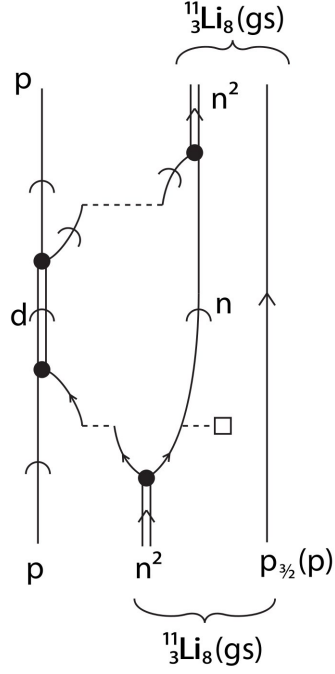


Figure 11. NFT diagrams summarizing the physics which is at the basis of the structure of  $^{11}\text{Li}$  [8] and of the analysis of the  $^{11}\text{Li}(p,t)^9\text{Li}(gs)$  reaction [26]. At variance with similar diagrams shown in Fig. 2 (c) and Fig. 3, in the present figure emphasis is set on intermediate (like e.g.  $^{10}\text{Li}+d$ , see (a) and (b)) and elastic (see (c), see also Fig. 12) channels.

## OPTICAL POTENTIAL



$$\begin{aligned}
 \sum_p(k, \omega) &= \sum_{int} \frac{V_{p,int}^2}{\hbar\omega - E_{int}} , \\
 &= \lim_{\Delta \rightarrow 0} \sum_{int} \frac{V_{p,int}^2}{(\hbar\omega - E_{int}) + i\Delta/2} , \\
 &= \Delta E_p(k, \omega) + iW_p(k, \omega) ,
 \end{aligned}$$

$$\Delta E_p(k, \omega) = \lim_{\Delta \rightarrow 0} \sum_{int} \frac{2(E - E_{int})V_{p,int}^2}{(\hbar\omega - E_{int})^2 + \left(\frac{\Delta}{2}\right)^2} ,$$

$$W_p(k, \omega) = \lim_{\Delta \rightarrow 0} \sum_{int} \frac{V_{p,int}^2}{(\hbar\omega - E_{int})^2 + \left(\frac{\Delta}{2}\right)^2} ,$$

$$\Delta E_p(k, \omega) = U_p(k, \omega) = \frac{\mathcal{P}}{\pi} \int \frac{W_p(k, \omega')}{\omega - \omega'} d\omega' .$$

Kramers–Krönig

Figure 12. NFT diagrams and summary of the expression (see e.g. [38] and refs. therein) entering in the calculation of one of the contributions (that associated with one-particle transfer and, arguably, the dominant one) to the  $^{11}\text{Li}+p$  elastic channel. The self-energy function is denoted  $\Sigma_p$ , while the real and imaginary parts are denoted  $\Delta E_p(= U_p)$  and  $W_p$  respectively, the subindex  $p$  indicating the incoming proton. These quantities are, in principle, a function of frequency and momentum.

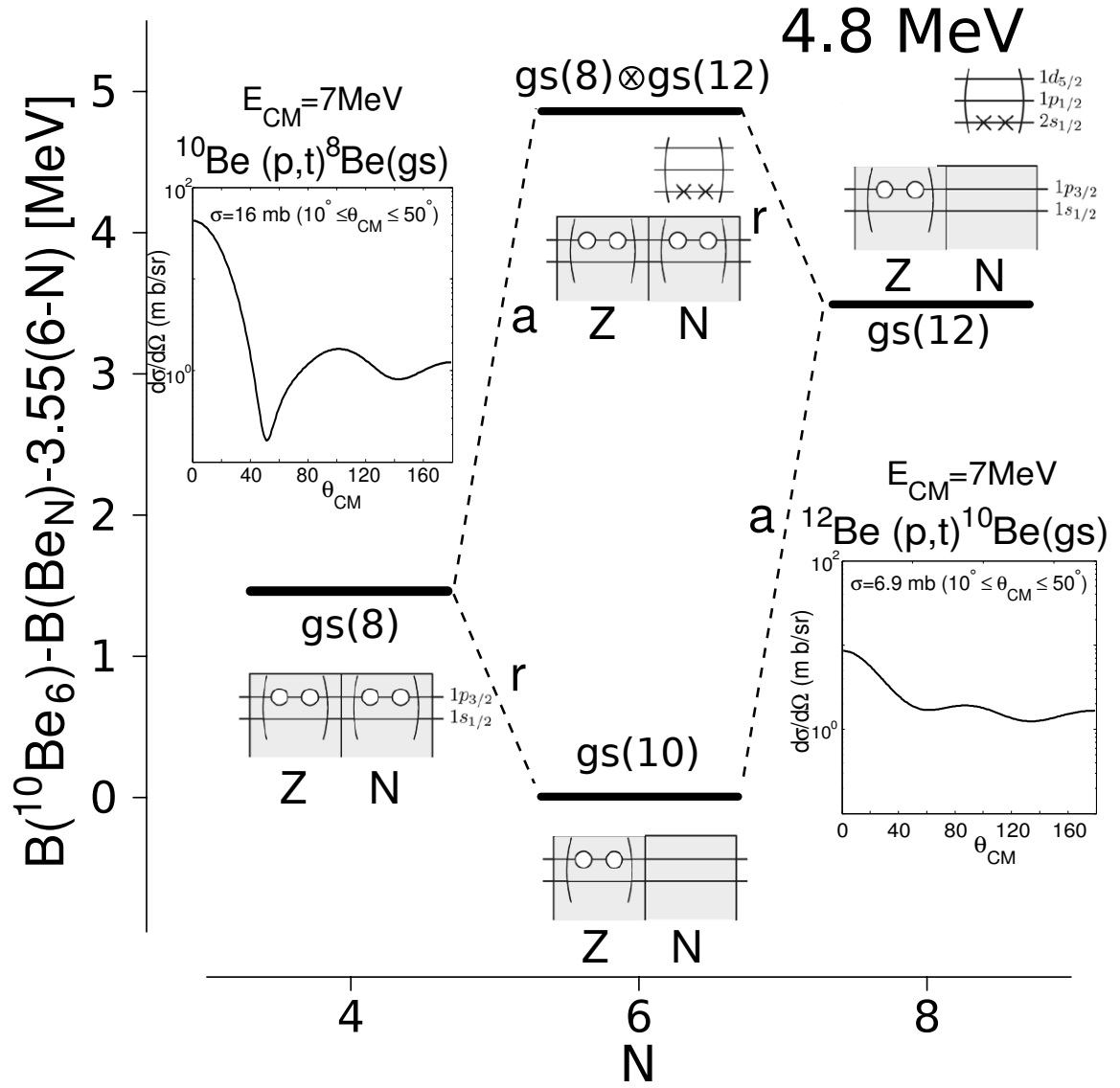


Figure 13. Pairing vibrational spectrum of  $\text{Be}_N$  (see also Fig. 21 below) and associated absolute two-nucleon transfer differential cross section calculated as explained in the text.



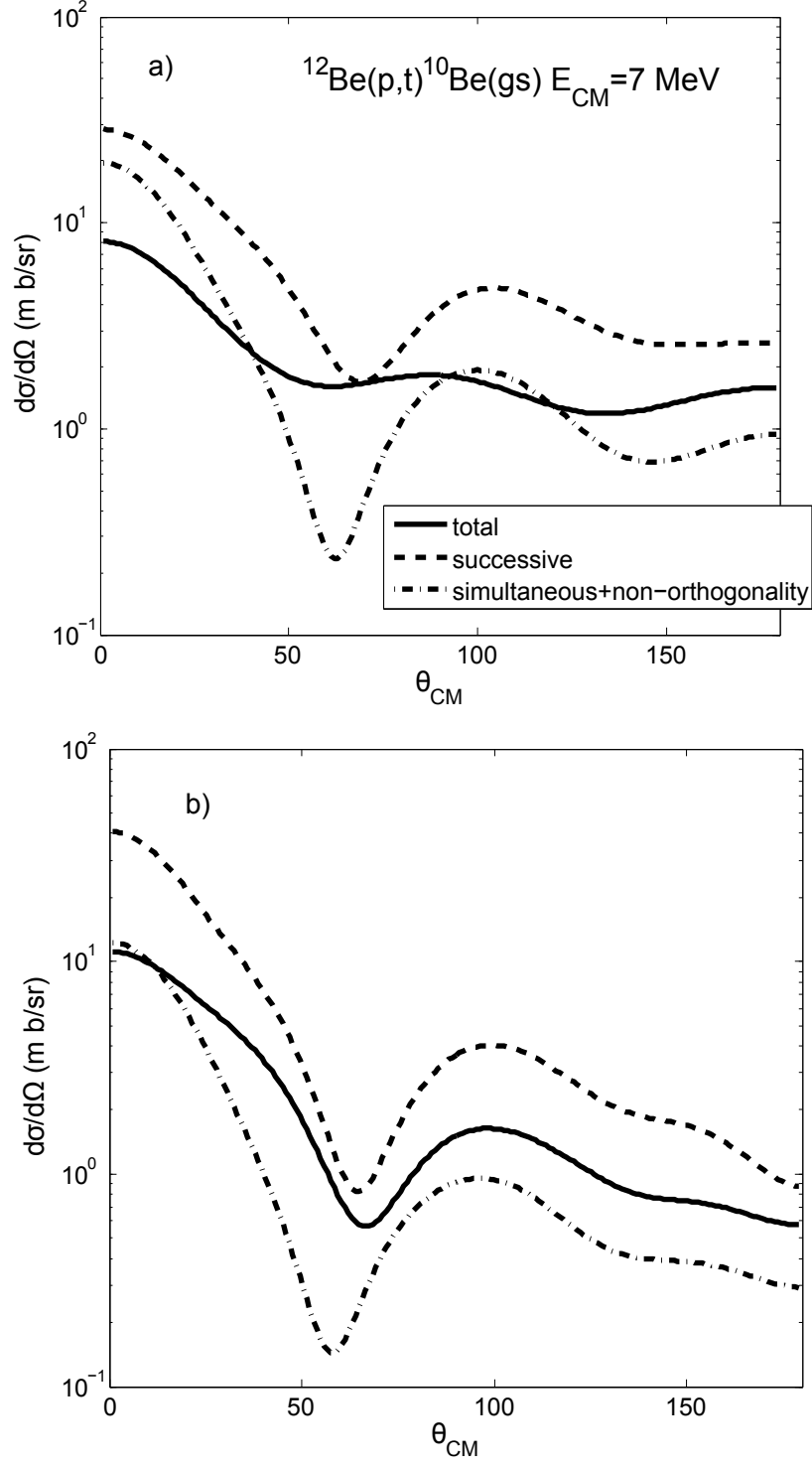


Figure 14. Absolute differential cross section associated with the reaction  $^{12}\text{Be}(p,t)^{10}\text{Be}(gs)$  at  $E_{CM} = 7$  MeV, calculated making use of : (a) the wavefunction (10) (already shown in Fig. 13) and (b), the RPA wavefunction describing the  $^{10}\text{Be}$  pair addition mode (see Table III).

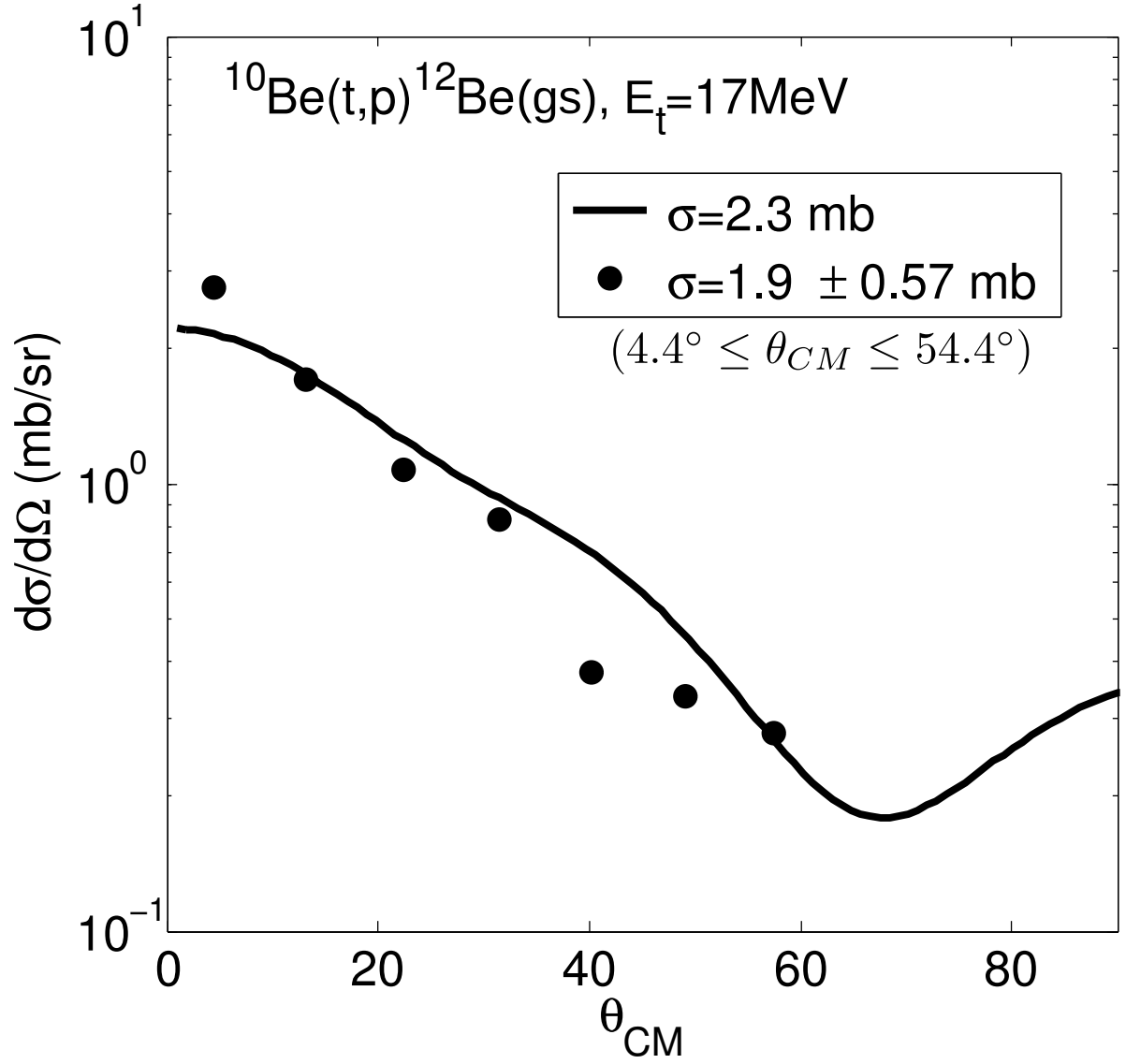


Figure 15. Absolute differential cross section measured [48] in the reaction  $^{10}\text{Be}(t,p)^{12}\text{Be}(gs)$  at 17 MeV triton bombarding energy (solid dots). The theoretical calculations (continuous solid curve) were obtained making use of the spectroscopic amplitudes associated with the wavefunction in Eqs. (10)-(12), and the optical parameters of refs. [37] and [48] taking into account successive, simultaneous and non-orthogonality processes.

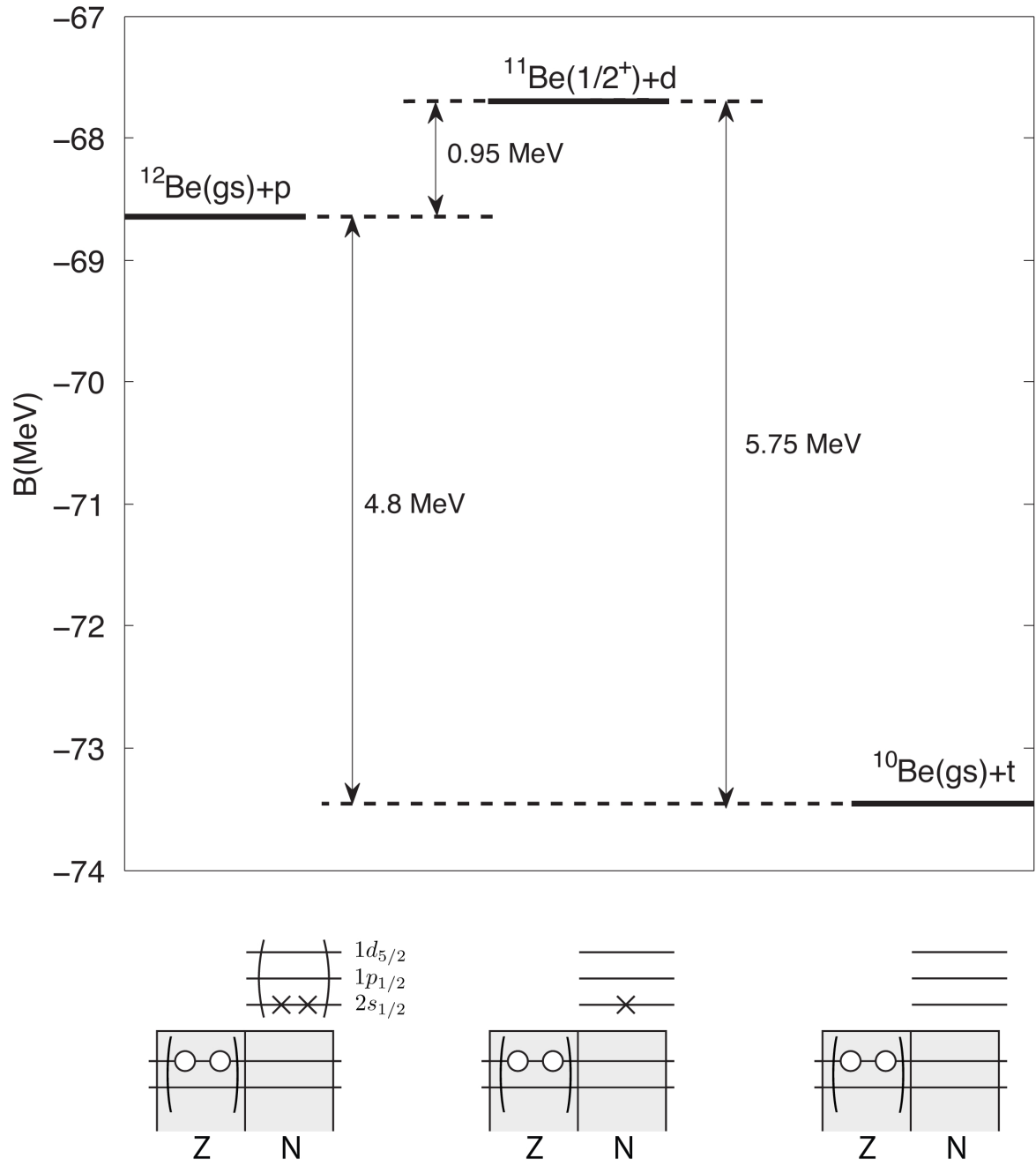


Figure 16. Q-values associated with the  $^{12}\text{Be}(p,t)^{10}\text{Be}(\text{gs})$ , also for the successive transfer (see text).

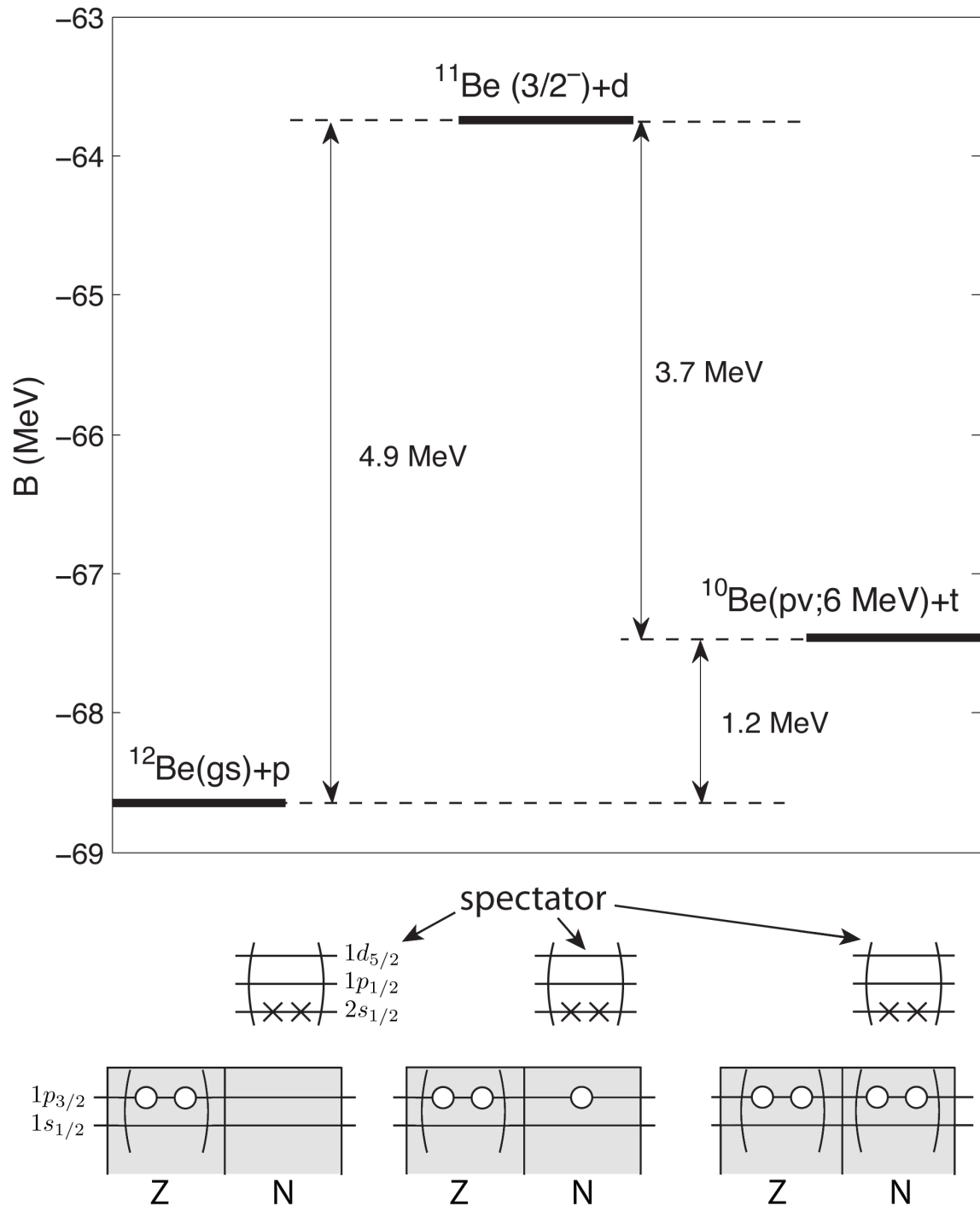


Figure 17. As for Fig. 16 but for the reaction  $^{12}\text{Be}(p, t)^{10}\text{Be}(pv; 6\text{MeV})$ .

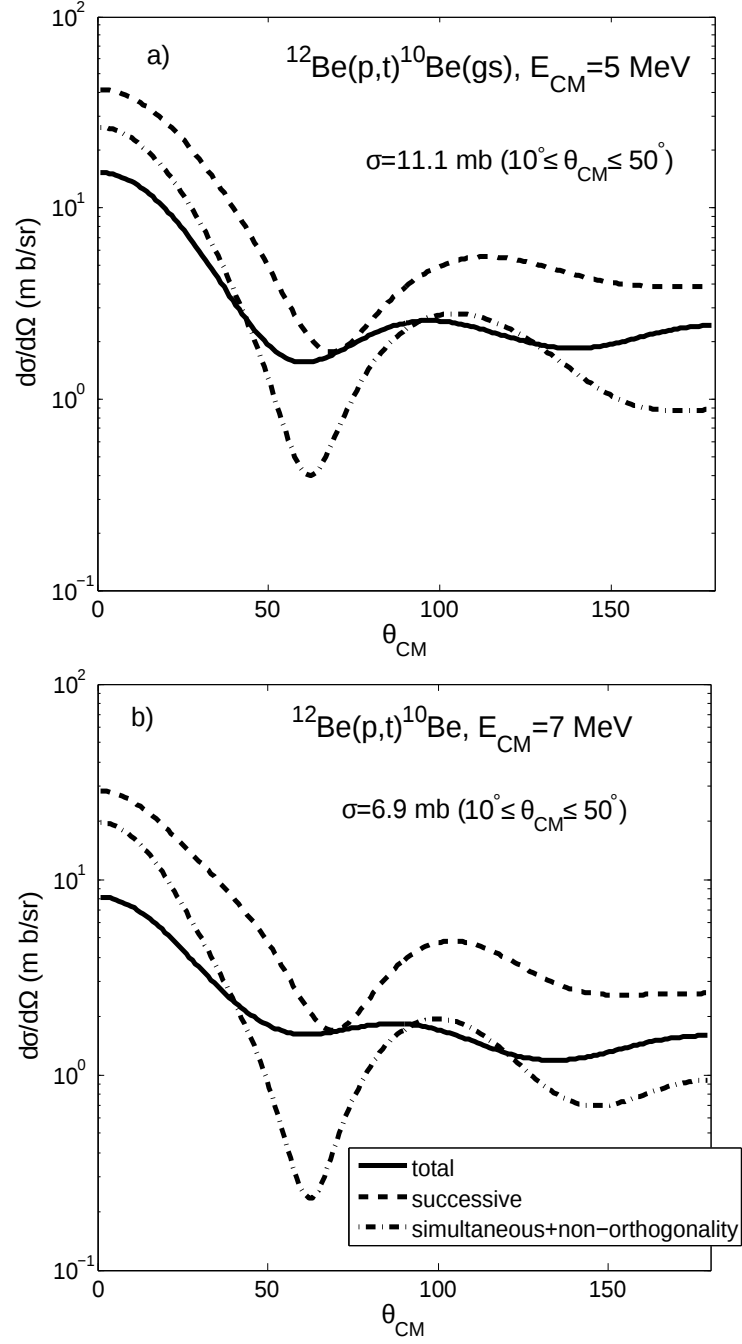


Figure 18. Absolute differential cross section associated with the reaction  $^{12}\text{Be}(p,t)^{10}\text{Be}(gs)$  at two bombarding energies (a) has already been displayed in Fig. 13). Also given are the integrated values of the cross section in the angular range  $10^\circ \leq \theta_{\text{CM}} \leq 50^\circ$ , as well as the different contributions to the total differential cross section.

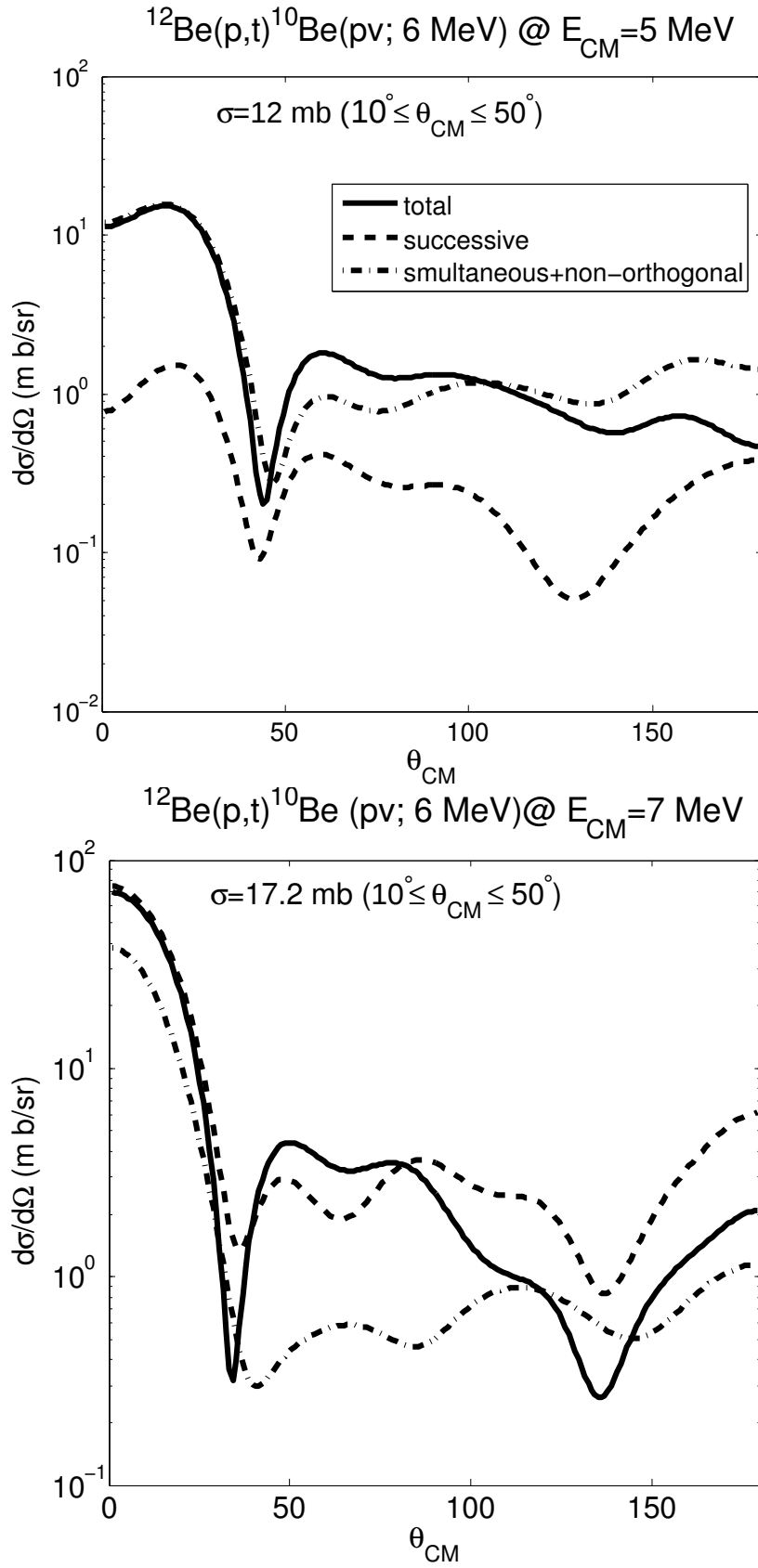


Figure 19. Absolute differential cross section associated with the reaction  $^{12}\text{Be}(p,t)^{10}\text{Be}(pv; 6\text{MeV})$  at two bombarding energies and integrated values of the cross section in the angular range  $10^\circ \leq \theta_{\text{CM}} \leq 50^\circ$ . Also displayed are the various contributions to the total differential cross section.

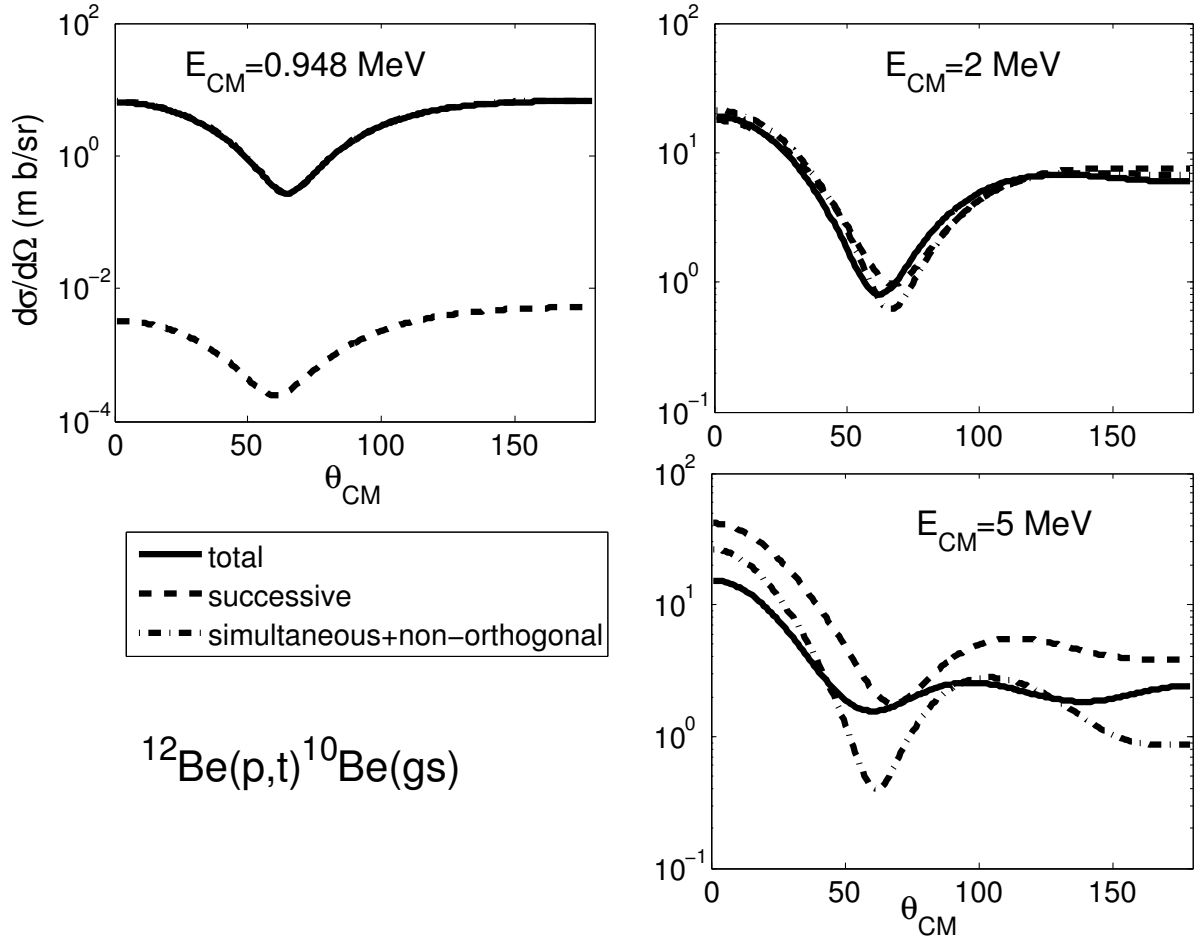


Figure 20. Absolute differential cross section associated with the reaction  $^{12}\text{Be}(p,t)^{10}\text{Be}(gs)$  at three bombarding energies. Also displayed are the various contributions to the total differential cross section.

	$1s_{1/2}$	$1p_{3/2}$		$1p_{1/2}$	$2s_{1/2}$
$\epsilon_i$ [MeV]	-16.07	-4.06	$\epsilon_k$ [MeV]	0.025	0.5
$X^r$	0.058	1.049	$Y^r$	0.244	0.211

Table I. RPA wavefunction of the pair removal mode of  ${}^9\text{Li}$ . Single-particle energies were deduced from experimental binding energy differences, while  $W_1(\beta = 2) = 3.36$  MeV,  $W_1(\beta = -2) = 2.3$  MeV. The results obtained making use of a single  $G$  or of two pairing coupling constants to take care of the difference of overlaps between core-core, core-halo and halo-halo single-particle wavefunctions are, in the present case, essentially the same (see App. A, in particular Sect. *b* of this appendix).

$$\sigma({}^{11}\text{Li}(\text{gs}) \rightarrow {}^9\text{Li}(\text{gs})) \text{ (mb)}$$

Theory	Experiment
6.1	$5.7 \pm 0.9$

$$\sigma({}^7\text{Li}(\text{gs}) \rightarrow {}^9\text{Li}(\text{gs})) \text{ (mb)}$$

14.3	$14.7 \pm 4.4$
------	----------------

Table II. Integrated two-neutron differential transfer cross sections, in the center of mass angular range  $20^\circ$ – $154.5^\circ$  for the reaction  ${}^{11}\text{Li}({}^1\text{H}, {}^3\text{H}){}^9\text{Li}(\text{gs})$  and in the center of mass angular range  $10^\circ$ – $109^\circ$  for the reaction  ${}^7\text{Li}(t, p){}^9\text{Li}(\text{gs})$  in which the measurements have been made, in comparison with the data ([34, 35]).

	$1s_{1/2}$	$1p_{3/2}$		$2s_{1/2}$	$1p_{1/2}$	$1d_{5/2}$
$\epsilon_k$ [MeV]	-19.55	-6.81	$\epsilon_i$ [MeV]	-0.50	-0.18	1.28
$X^r$	0.128	1.076	$Y^r$	0.232	0.214	0.272
$Y^a$	0.080	0.402	$X^a$	0.727	0.588	0.543

Table III. RPA wavefunctions of pair removal and addition  $0^+$  modes of  ${}^{10}\text{Be}$ , that is, of the ground state of  ${}^8\text{Be}$  and  ${}^{12}\text{Be}$ . The single-particle energies were deduced from experimental binding and excitation energies, and making use of the coupling constants  $G_{cc} = 2$  MeV and  $G_{hc} = G_{hh} = 0.68$  MeV (see App. A, in particular Sect. *b*).



	$\varepsilon_i$ [MeV]	$\varepsilon_k$ [MeV]	$E$ [MeV]	X	Y
n	$p_{3/2}$ -8.6	$p_{1/2}$ -3.6	5.0	0.90	0.31
p	$p_{3/2}$ -14.9	$p_{3/2}$ -14.9	7.6	-0.56	-0.29
p	$p_{3/2}$ -14.9	$p_{1/2}$ -7.8	12.2	0.24	0.16
n	$p_{3/2}$ -8.6	$f_{7/2}$ 16.5	25.1	-0.12	-0.10
p	$s_{1/2}$ -29.0	$d_{5/2}$ -1.6	28.4	-0.10	-0.08
n	$p_{3/2}$ -8.6	$f_{7/2}$ 8.8	17.5	-0.10	-0.07
n	$s_{1/2}$ -21.1	$d_{5/2}$ 2.2	28.4	-0.09	-0.07

Table IV. Wavefunction of the lowest  $2^+$  vibrational state (phonon) of  $^{10}\text{Be}$  (obtained from a QRPA calculation, making use of a quadrupole separable interaction and a value of the proton pairing gap of  $\Delta_p = 3.8$  MeV while setting  $\Delta_n = 0$ ). The calculated energy and the  $B(E2)$  transition strength of the low lying  $2^+$  are 2.5 MeV and  $49.6 e^2\text{fm}^4$  respectively. These results are to be compared with the experimental values of 3.3 MeV and  $52 e^2\text{fm}^4$ . The quantities  $\varepsilon_i$  and  $\varepsilon_k$  indicate the energy of the hole and of the particle states respectively for either protons (p) or neutrons (n).  $E$  denotes the associated two-quasiparticle energies, while  $X$  and  $Y$  are the QRPA amplitudes of the mode.

## Appendix A: Pairing and surface vibrations for pedestrians

A pairing vibration is a harmonic mode which changes the number of particles in  $+2$  or  $-2$ , and can be observed, around closed shell nuclei, as strong transitions in two-particle transfer processes. For example around  $^{208}\text{Pb}$ , where the monopole, pair addition mode (a) is the ground state of  $^{210}\text{Pb}$  and the pair removal mode (r) is the ground state of  $^{206}\text{Pb}$  [4]. The two-phonon pairing vibration of  $^{208}\text{Pb}$  ( $^{208}\text{Pb}(pv; 0^+, 4.9 \text{ MeV})$ ) is thus a two-particle two-hole state, product of these two ground states, and thus expected, in the harmonic approximation, at an energy of 4.9 MeV above the  $^{208}\text{Pb}$  ground state (see [1] and refs. therein, see also [18]). Consequently, and within the harmonic approximation, in the reaction  $^{206}\text{Pb}(t, p)^{208}\text{Pb}(pv)$  one excites the pair addition mode, with quite similar ( Q-value, angular distribution, cross section, etc. ) observables to those associated with the  $^{208}\text{Pb}(t, p)^{210}\text{Pb}(gs)$  reaction. Of notice that the pair addition mode  $|gs(^{210}\text{Pb})\rangle$  can be viewed as a correlated two-particle state, linear combination of  $(j^2(0))^2$  configurations,  $j$  denoting valence orbitals ( $2g_{9/2}$ ,  $1i_{11/2}$ ,  $3d_{5/2}$ , ...) lying above the Fermi energy. Now, because of ground state correlations, the (RPA) wavefunction of the pair addition mode contains also components of the type  $(j^{-2}(0))$ , i.e. corresponding to the correlation of two-hole-states in the occupied valence orbitals lying below the Fermi energy ( $3p_{1/2}$ ,  $2f_{5/2}$ ,  $3p_{3/2}$ , ...). These correlations add coherently to the previous ones in binding the two neutrons (Cooper pair partners) of the pair addition mode to the  $^{208}\text{Pb}$  core. Similar arguments apply to the removal mode, but where the role of holes and particles are exchanged. For an example see Table III, where the two-nucleon transfer spectroscopic amplitudes (see e.g. App. 2, ref. [4]), proportional to the RPA wavefunction amplitudes of  $^{10}\text{Be}$ , are collected. In the case of  $^{10}\text{Be}$  one expects the two-phonon pairing vibrational 2p-2h state at an energy of 4.8 MeV above the ground state <sup>5</sup>, an energy which emerges directly from two differences in binding energies, namely  $[(BE(^{10}\text{Be}) - BE(^8\text{Be})) - [BE(^{12}\text{Be}) - BE(^{10}\text{Be})]] = 4.8 \text{ MeV}$  (see Fig. 21; see also Fig 13 where the same spectrum is displayed, but subtracting to  $BE(^{10}\text{Be})) - (BE(^4\text{Be}_N)$  a linear term in  $N$ , i.e. essentially eliminating the A-dependent term of Weiszäcker mass formula, so as to be able to compare the excitation energies of  $^8\text{Be}(gs)$  and  $^{12}\text{Be}(gs)$  with respect to  $^{10}\text{Be}(gs)$ .

In the reaction  $^{210}\text{Pb}(p, t)^{208}\text{Pb}$  one would also excite, for example, the particle-hole

---

<sup>5</sup> It is of notice the totally accidental similarity between the harmonic predicted value of the two-phonon pairing vibrational state in  $^{208}\text{Pb}$  (4.9 MeV) and in  $^{10}\text{Be}$  (4.8 MeV).

quadrupole vibrational state of  $^{208}\text{Pb}$ , that is  $^{210}\text{Pb}(p, t)^{208}\text{Pb}(2^+; 4.07\text{MeV})$ ,  $2^+$  which decays electromagnetically to the ground state of  $^{208}\text{Pb}$  with a  $B(E2)$  value corresponding to approximately 5 Weisskopf single-particle units. On one hand this state, which is very interesting by itself (in particular when exchanged between the two outer neutrons in the  $^{210}\text{Pb}$  ground state, it contributes to the pairing correlations of the pair addition mode), has nothing to do with the pairing vibrational spectrum, in the same way in which the  $2^+$  state of  $^{10}\text{Be}$  is not related to the pairing spectrum around magic number  $N = 6$ . On the other hand, the residual interaction correlating the particle and the hole (linear combination of particle-hole excitations  $(j_k, j_i^{-1})_{2+}$  of the quadrupole vibration) pulls the hole close to the particle. This is reason why collective surface vibrations display both enhanced electromagnetic transition probabilities, i.e.  $B(E\lambda)$  values, and enhanced two-nucleon transfer cross section. The main difference between surface ((p-h)-like) vibrational modes and pairing vibrational modes lies, as far as two-nucleon transfer processes are concerned, in the role played by the ground state correlations. While those associated with the pair addition and pair subtraction modes enhance the two-nucleon transfer cross sections, those associated with particle-hole excitations, while increasing the electromagnetic decay probabilities, decrease the two-nucleon transfer cross section (see e.g. [49, 50]). This competition between ((pp)-(hh))- and (ph)- ground state correlations in nuclei, is at the basis of the studies of pairing in nuclei in terms of the competition between deformed and spherical shapes (see e.g. [14, 51–53] and Fig. 22).

*a. Calculation of energy and wavefunctions of pairing vibrations*

The two-phonon,  $0^+$  of pairing vibrational state, of the closed shell system  $N_0$  can be written, in the harmonic approximation as (cf. [1] Ch. 5, see also [4, 18] and refs. therein)

$$|pv\rangle = |gs(N_0 + 2)\rangle |gs(N_0 - 2)\rangle, \quad (\text{A1})$$

where

$$|gs(N_0 + 2)\rangle = \Gamma_1^\dagger(\beta = +2)|0\rangle, \quad (\text{A2})$$

and

$$|gs(N_0 - 2)\rangle = \Gamma_1^\dagger(\beta = -2)|0\rangle, \quad (\text{A3})$$

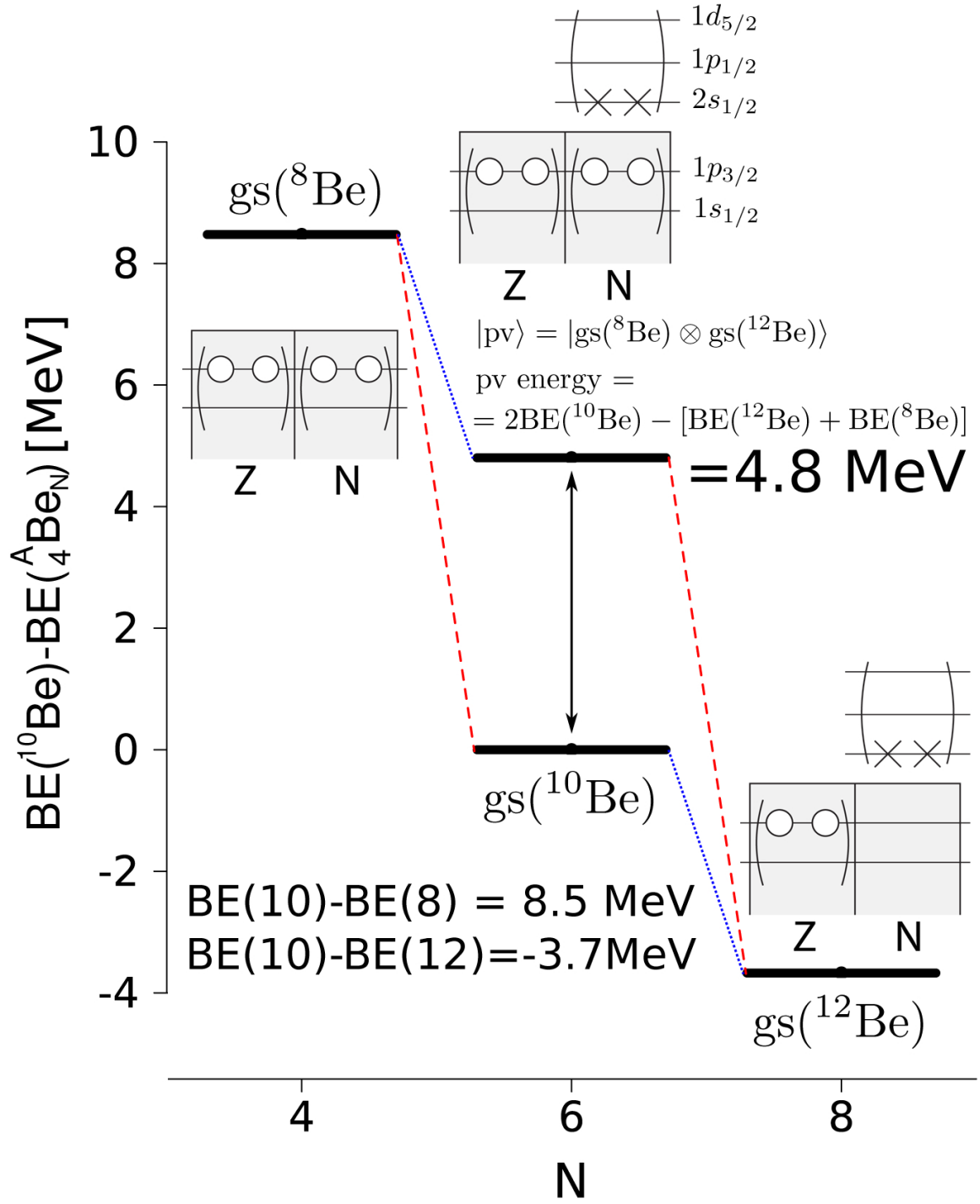


Figure 21. In the harmonic approximation, the two-phonon pairing vibration state of  $^{10}\text{Be}$  is the state  $|gs(^8\text{Be}) \otimes gs(^{12}\text{Be})\rangle$ , its energy being given by the sum of the relative binding energies (BE) of  $^8\text{Be}$  and  $^{12}\text{Be}$  as indicated (see also Fig. 13).

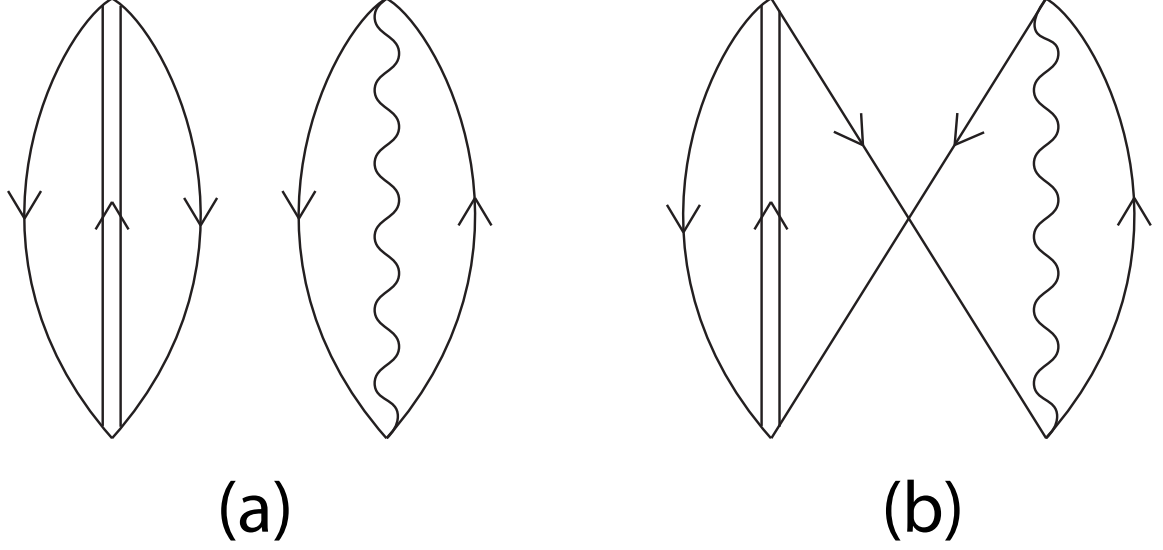


Figure 22. (a) Zero Point Fluctuations (ZPF) associated with a pair addition mode and a surface ((p-h)-like) vibration. (b) Pauli principle correction of (pp)-like ZPF in presence of (ph)-like ZPF.

are the RPA ground state correlated states of the  $N_0 + 2$  and the  $N_0 - 2$  system respectively. The pair addition and pair removal creation operator phonons are written as

$$\Gamma_n^\dagger(\beta = +2)|0\rangle = \sum_k X_n^a(k)\Gamma_k^\dagger + \sum_i Y_n^a(i)\Gamma_i, \quad (\text{A4})$$

where

$$\Gamma_k^\dagger = [a_k^\dagger a_k^\dagger]_0, \quad (\text{A5})$$

creates a pair of particles coupled to angular momentum zero in levels with energy  $\varepsilon_k > \varepsilon_F$  ( $k \equiv n_k l_k j_k$ ), while

$$\Gamma_i = [a_i a_i]_0, \quad (\text{A6})$$

creates a pair of holes in the occupied orbitals, i.e. orbitals with energy  $\varepsilon_i \leq \varepsilon_F$  ( $i \equiv n_i l_i j_i$ ). The index  $n(=1, 2, \dots)$  labels the lowest, the first excited, etc. states. In what follows we concentrate on the  $n = 1$  (ground) modes, otherwise explicitly mentioned.

Assuming  $\Gamma_k^\dagger$  and  $\Gamma_i^\dagger$  display boson commutation relations, one can linearize the pairing Hamiltonian obtaining the dispersion relation for the lowest ( $n = 1$ ) modes (see Fig. 23 for the case of the pairing vibrational spectrum around  $^{10}\text{Be}$ )

$$S(\beta = \pm 2) = \frac{1}{G(\beta = \pm 2)}, \quad (\text{A7})$$

where (note that  $\beta = \pm 2$  is simplified in what follows into  $\pm 2$ ),

$$S(\pm 2) = S_h(\pm 2) + S_c(\pm 2), \quad (\text{A8a})$$

with

$$S_h(\pm 2) = \sum_k \frac{\Omega_k}{2(\varepsilon_k - \varepsilon_F) \mp W_1(\pm 2)} \quad (\text{A8b})$$

and

$$S_c(\pm 2) = \sum_i \frac{\Omega_i}{2(\varepsilon_F - \varepsilon_i) \pm W_1(\pm 2)} \quad (\text{A9})$$

while  $\Omega = j + 1/2$  measure the pair degeneracy of the single particle orbital  $j$ .

The RPA amplitudes appearing in (A4) are defined as

$$X_1^a(k) = \frac{\frac{1}{2}\sqrt{\Omega_k} \Lambda_1(+2)}{2(\varepsilon_k - \varepsilon_F) - W_1(+2)} \quad , \quad Y_1^a(i) = -\frac{\frac{1}{2}\sqrt{\Omega_i} \Lambda_1(+2)}{2(\varepsilon_F - \varepsilon_i) + W_1(+2)}, \quad (\text{A10a})$$

and

$$X_1^r(i) = \frac{\frac{1}{2}\sqrt{\Omega_i} \Lambda_1(-2)}{2(\varepsilon_F - \varepsilon_i) - W_1(-2)} \quad , \quad Y_1^r(k) = -\frac{\frac{1}{2}\sqrt{\Omega_k} \Lambda_1(-2)}{2(\varepsilon_k - \varepsilon_F) + W_1(-2)}, \quad (\text{A10b})$$

The particle-vibration coupling strengths  $\Lambda_1(\beta = \pm 2)$  are determined from the normalization conditions

$$\sum_k |X_1^a(k)|^2 - \sum_i |Y_1^a(i)|^2 = 1, \quad (\text{A11})$$

and

$$\sum_i |X_1^r(i)|^2 - \sum_k |Y_1^r(k)|^2 = 1, \quad (\text{A12})$$

respectively.

*b. Extension of the harmonic approximation to the case of more than one pairing coupling constant*

The relation between the pairing coupling constant  $G$  and the matrix elements between pure two-particle configurations  $(j^2)_0$  coupled to angular momentum  $J = 0$ , of a  $\delta$ -force of strength  $V_0$  can be written as (see e.g. Eq. (2-24) p.41 ref. [1]),

$$G = V_0 I, \quad (\text{A13})$$

where

$$I = \int dr \, r^2 \mathcal{R}_f^2(r) \mathcal{R}_i^2(r), \quad (\text{A14})$$

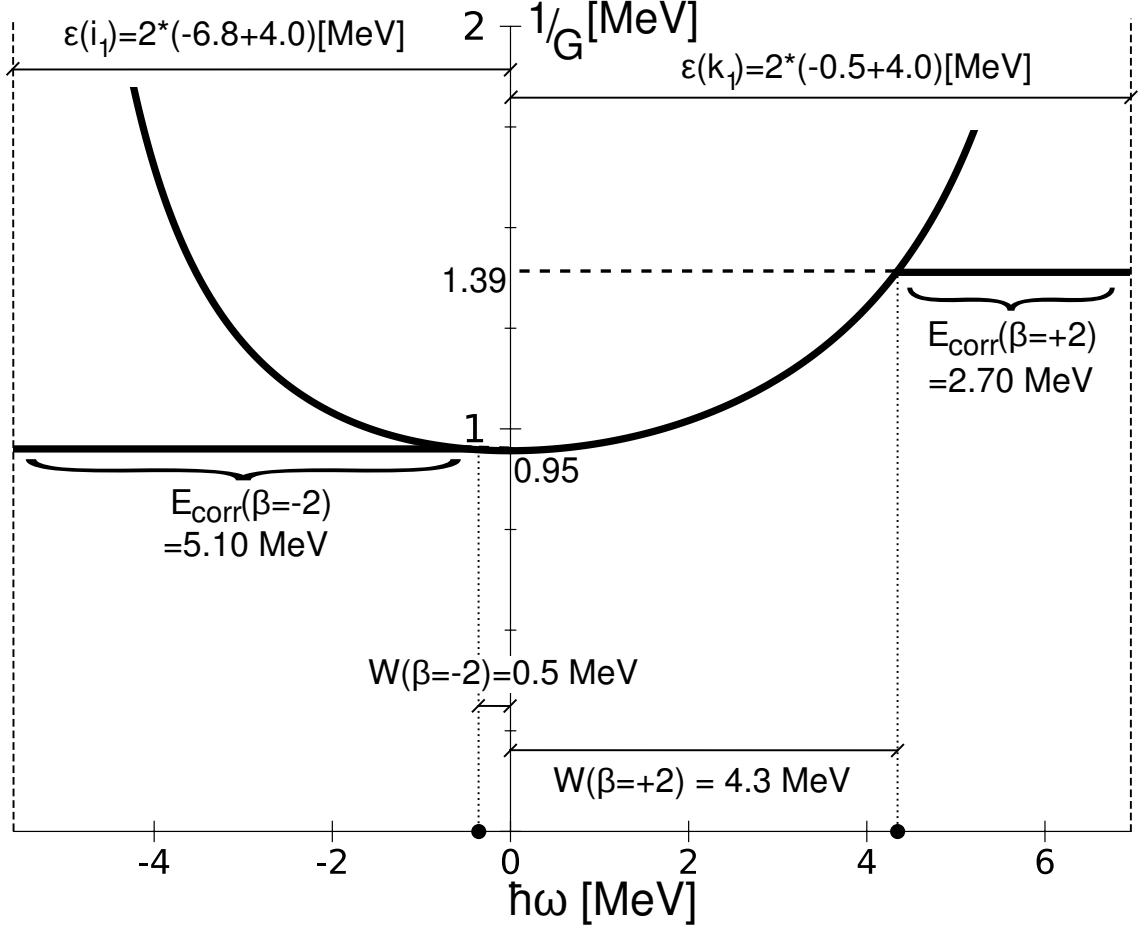


Figure 23. Dispersion relation and parameters characterizing the pairing vibrational spectrum of  $^{10}\text{Be}$ . The quantity  $E_{\text{corr}}(\beta = +2) = (BE(^{12}\text{Be}) - BE(^{10}\text{Be})) - 2(BE(^{11}\text{Be}) - BE(^{10}\text{Be})) = (68.7 - 65.0) - 2(65.5 - 65.0) = 2.7$  MeV while  $W_1(\beta = +2) = 2\varepsilon(k_1) - E_{\text{corr}}(\beta = +2) = 2(-0.5 + 4.0) - 2.7 = 4.3$  MeV, with  $\varepsilon(k_1) = S_n(^{11}\text{Be}) - \varepsilon_F = -0.5 + 4.0$  MeV,  $S_n(^{11}\text{Be})$  being the experimental neutron separation energy in  $^{11}\text{Be}$ . Thus  $\varepsilon(k_1)$  is the energy of the first unoccupied state of  $^{11}\text{Be}$ , calculated respect to the Fermi energy  $\varepsilon_F = -4.0$  MeV (for details see App. B). Similar expressions are valid for the pair removal mode, namely  $E_{\text{corr}}(\beta = -2) = 5.10$  MeV,  $W_1(\beta = -2) = -2\varepsilon(i_1) - E_{\text{corr}}(\beta = -2) = 0.5$  MeV, where  $\varepsilon(i_1) = -6.8 + 4.0$  MeV is the energy of the first occupied state respect to the Fermi energy. The inverse strengths  $1/G(\pm 2)$  intersect the dispersion relation at values of  $\hbar\omega$  leading to  $W_1(\beta = \pm 2)$ .

$\mathcal{R}$  being the radial single-particle wavefunction describing initial ( $i$ ) and final ( $f$ ) configurations. Making use of the approximation (constant value of  $\mathcal{R}$  inside the nucleus of radius  $R$ ),

$$\mathcal{R} = \sqrt{\frac{3}{R^3}} \Theta(r - R), \quad (\text{A15})$$

where

$$\Theta(r - R) = 1 \quad (r \leq R) \quad ; \quad \Theta(r - R) = 0 \quad (r > R), \quad (\text{A16})$$

one can write

$$I_{if} = \frac{R_j^3}{3} \frac{3}{R_f^3} \frac{3}{R_i^3}, \quad (\text{A17})$$

$R_j$  being equal to the smallest value of the radius  $R_i$  and  $R_f$ .

A simple estimate of  $V_0$  can be worked out assuming  $R_i = R_f = R$ , and using the standard expression for the pairing coupling constant  $G \approx 25/A$  MeV. One thus obtains

$$4\pi V_0 = \frac{25 \text{ MeV}}{\rho_0} \approx 150 \text{ MeV fm}^3, \quad (\text{A18})$$

where  $\rho_0 = A/\text{Vol} \approx 0.17 \text{ fm}^{-3}$  ( $\text{Vol} = 4\pi/3 R^3$ ), corresponds to the nuclear saturation density .

Distinguishing between core ( $c$ ) and halo ( $h$ ) single-particle wavefunctions and thus radii, one obtains two different expressions for (A17), namely

$$I_{cc} = \frac{4\pi}{\text{Vol}(c)}, \quad (\text{A19})$$

and

$$I_{hh} = I_{hc} = \frac{4\pi}{\text{Vol}(h)}. \quad (\text{A20})$$

Making use of Eq. (A18) one can write

$$G_{cc} = \frac{150 \text{ MeV fm}^3}{\text{Vol}(c)} \quad (\text{A21})$$

and

$$G_{hh} = G_{hc} = \frac{150 \text{ MeV fm}^3}{\text{Vol}(h)}. \quad (\text{A22})$$

Using the parametrization of the nuclear radius according to Eq. (2-181) of ref. [31], one obtains  $R_c = 1.27 \times 8^{1/3} \text{ fm} = 2.54 \text{ fm}$ . leading to  $\text{Vol}(c) \approx 70 \text{ fm}^3$ . Thus

$$G_{cc} \approx 2 \text{ MeV}. \quad (\text{A23})$$



Let us now carry out a simple estimate of  $G_{hh}$ , assuming that  $R_h$  is about 35% larger than  $R_c$ , a value in line with the observations in light halo nuclei. In this case,  $\text{Vol}(h) \approx 170\text{fm}^3$ . Thus

$$G_{hh} = G_{hc} \approx 0.9 \text{ MeV}. \quad (\text{A24})$$

In the present case one can distinguish three terms in the pairing Hamiltonian, namely

$$H_p = H_p(h) + H_p(c) + H_p(hc), \quad (\text{A25})$$

where

$$H_p(h) = -G_{hh} \sum_{\substack{k, k' \\ \varepsilon_k, \varepsilon_{k'} > \varepsilon_F}} a_k^\dagger a_{\bar{k}}^\dagger a_{k'} a_{\bar{k}'}, \quad (\text{A26})$$

$$H_p(c) = -G_{cc} \sum_{\substack{i, i' \\ \varepsilon_i, \varepsilon_{i'} \leq \varepsilon_F}} a_i^\dagger a_{\bar{i}}^\dagger a_{i'} a_{\bar{i}'}, \quad (\text{A27})$$

and

$$H_p(hc) = -G_{ch} \sum_{k, i} (a_k^\dagger a_{\bar{k}}^\dagger a_{\bar{i}} a_i + a_i^\dagger a_{\bar{i}}^\dagger a_{\bar{k}} a_k). \quad (\text{A28})$$

Linearizing these equations one obtains, instead of the dispersion relation (A7), the determinant (within this *formal* context see e.g. App J of ref. [1])

$$\begin{vmatrix} 1 - G_{hh}S_h(\pm 2) & G_{hc}S_c(\pm 2) \\ G_{hc}S_h(\pm 2) & 1 - G_{cc}S_c(\pm 2) \end{vmatrix} = 0, \quad (\text{A29})$$

and in the amplitudes (A.10) the substitutions of  $\Lambda_1(+2)$  and  $\Lambda_1(-2)$  by

$$G_{hh}A + G_{hc}B, \quad (\text{A30a})$$

and

$$G_{cc}C + G_{hc}D, \quad (\text{A30b})$$

respectively are to be made ( $A = \sum_k X_1^a(k)$ ,  $B = \sum_i Y_1^a(i)$ ,  $C = \sum_i X_1^r(i)$  and  $D = \sum_k Y_1^r(k)$ ). It is of notice that, in the case in which  $G_{cc} = G_{hh} = G_{hc} = G$ , (A29) becomes

$$1 - G(S_h(\pm 2) + S_c(\pm 2)) = 1 - GS(\pm 2) = 0, \quad (\text{A31})$$

while (A30a) and (A30b) coincide with  $\Lambda_1(+2)$  and  $\Lambda_1(-2)$  respectively.

While the results obtained by parametrizing the pair addition and pair removal modes in terms of  $G_{hh} = G_{hc}$  and  $G_{cc}$  are very different from those using a single  $G$  in the case of  $^{10}\text{Be}$

	$1s_{1/2}$	$1p_{3/2}$		$2s_{1/2}$	$1p_{1/2}$	$1d_{5/2}$
$\epsilon_k$ [MeV]	-19.55	-6.81	$\epsilon_i$ [MeV]	-0.50	-0.18	1.28
$X_r$	0.237	1.993	$Y_r$	0.969	0.892	1.137
$Y_a$	0.053	0.264	$X_a$	0.699	0.563	0.517

Table V. RPA amplitudes associated with the pair addition and removal modes of  $^{10}\text{Be}$ . The calculation were carried making use of a single pairing coupling constant for the pair addition mode ( $G = 0.72$  MeV) and for the pair removal mode ( $G = 1.053$  MeV).

pair removal mode, they lead to rather similar results in the case of pair addition mode (see Tables III and V). This is connected with the fact that the pair addition mode is mainly built on halo-like orbitals. The differences found between the results of the two calculations in the case of the pair addition and removal modes of  $^9\text{Li}$  (namely  $^{11}\text{Li}(gs)$  and  $^7\text{Li}(gs)$ ) is quite small. This is keeping with the fact that in this case the  $d_{5/2}$  orbital plays a rather minor role in the halo component of the corresponding wavefunctions. In other words, the basic halo subspace more than doubles going from Li ( $s_{1/2}, p_{1/2}$ ) to Be( $s_{1/2}, p_{1/2}, d_{5/2}$ ). Returning to the pair removal mode of  $^{10}\text{Be}$ , it is seen from Fig. 25, that the predicted absolute cross section associated with the reaction  $^{10}\text{Be}(p, t)^8\text{Be}(gs)$  ( $E_{CM} = 7$  MeV) and the integrated between  $10^\circ$  and  $50^\circ$  increases, from the value of 16 mb, to an (unrealistic) value close to the geometric cross section ( $\sigma = \pi R^2(^{10}\text{Be}) \sim \pi(2.5180 \pm 0.0114 fm)^2 \approx 200\text{mb}$ ).

## Appendix B: Fermi energy and Fermi level (chemical potential)

The Fermi energy  $\varepsilon_F$  is the energy of the highest occupied state in a macroscopic ("infinite") system of non-interacting fermions. Under these conditions it is the increase in the ground state energy when one particle is added to the system. At zero temperature it coincides with the chemical potential (Fermi level).

The situation is somewhat more subtle in the case of a finite, many-body system, like the atomic nucleus (see e.g. [38, 44] and refs. therein), as spatial quantization leads to a discrete spectrum. In this case it is useful to refer to the properties of the one-body Green

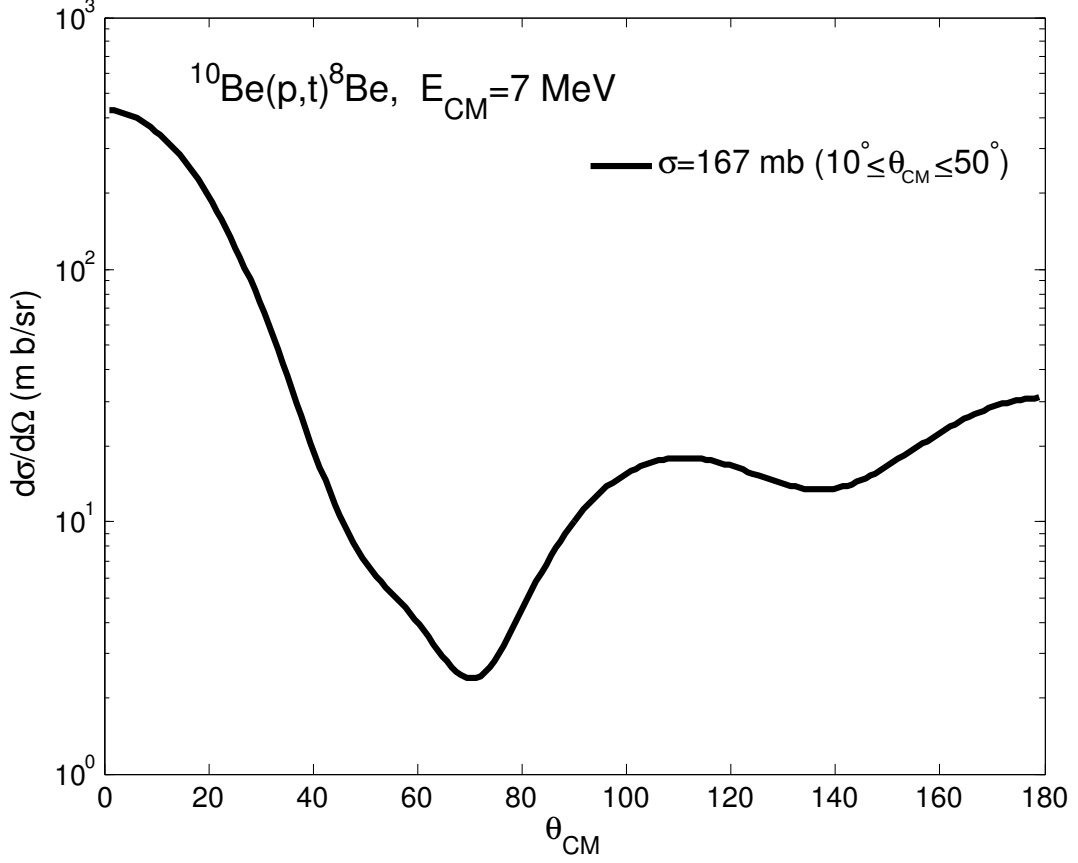


Figure 24. Absolute differential cross section associated with the reaction  $^{10}\text{Be}(p,t)^8\text{Be}(gs)$  at  $E_{CM} = 7$  MeV making use of the spectroscopic amplitudes calculated making use of a single pairing coupling constant (see Table V).

function (e.g. in the Lehmann representation)

$$G(\vec{r}, \vec{r}'; \omega) = \sum_i \frac{\varphi_i(\vec{r}) \varphi_i^*(\vec{r}')}{\omega - \omega_i - i\eta} + \sum_k \frac{\varphi_k(\vec{r}) \varphi_k^*(\vec{r}')}{\omega - \omega_k - i\eta}, \quad (\text{B1})$$

where

$$\varphi_i(\vec{r}) = \langle \psi_i^{(A-1)} | a(\vec{r}) | \psi_0^{(A)} \rangle, \quad (\text{B2})$$

and

$$\varphi_k(\vec{r}) = \langle \psi_0^{(A)} | a(\vec{r}) | \psi_i^{(A+1)} \rangle. \quad (\text{B3})$$

Here  $\psi_i^{(A-1)}$  is an eigenstate of the Hamiltonian describing the  $(A-1)$  particle system, with energy  $E_i^{A-1}$ ,  $\psi_k^{A-1}$  being eigenstate of the  $(A+1)$ -particle system with energy  $E_k^{(A+1)}$  and

$$\omega_k = E_k^{(A+1)} - E_0^{(A)}, \quad \omega_i = E_0^{(A)} - E_i^{(A-1)}, \quad (\text{B4})$$

where  $E_0^{(A)}$  is the energy of  $\psi_0^{(A)}$ . Closure relations yield

$$\sum_k \varphi_k(\vec{r}) \varphi_k^*(\vec{r}') + \sum_i \varphi_i(\vec{r}) \varphi_i^*(\vec{r}') = \delta(\vec{r} - \vec{r}'). \quad (\text{B5})$$

The analytic properties of  $G(\vec{r}, \vec{r}'; \omega)$  in the complex  $\omega$ -plane are schematically represented in Fig. 25. The one-body Green function has a right-hand cut which runs below the real  $\omega$ -axis between  $\omega = \varepsilon_t^+$  and  $\omega = +\infty$ . Here,  $\varepsilon_t^+$  is the energy ( $\varepsilon(k_2) - \varepsilon_F$ ) of the lowest excited state  $k_2$  of the  $(A+1)$  system measured with respect to  $\varepsilon_F = (\varepsilon_F^+ + \varepsilon_F^-)/2 = (E_0^{(A+1)} - E_0^{(A-1)})/2$  (see (B7) and (B9) below), that is, it is the threshold energy of the first inelastic channel. It is of notice that  $\varepsilon(k_2)$  is equal to  $-3.25$  MeV and  $-0.18$  MeV in the case of  $^{208}\text{Pb}$  and  $^{10}\text{Be}$  respectively. The one-body Green function has a left-hand cut which runs above the real  $\omega$ -axis and extends from  $-\infty$  to  $\varepsilon_t^-$  with

$$\varepsilon_t^- = E_0^{(A)} - E_0^{(A-2)}. \quad (\text{B6})$$

The left-hand cut corresponds to the possibility of the decay of the  $(A-1)$  into the  $(A-2)$  nucleus. The one-body Green function has discrete poles  $\omega_i$  between  $\varepsilon_t^+$  and  $\varepsilon_F^-$ , where

$$\varepsilon_F^- = E_0^{(A)} - E_0^{(A-1)}. \quad (\text{B7})$$

These poles correspond to bound states of the  $(A-1)$  nucleus with excitation energy

$$E_x^{(A-1)} = \varepsilon_F^- - \omega_i. \quad (\text{B8})$$

The Green function has also poles  $\omega_k$  on the real axis between  $\omega = \varepsilon_F^+$  and  $\omega = 0$ , where

$$\varepsilon_F^+ = E_0^{(A+1)} - E_0^{(A)}. \quad (\text{B9})$$

These correspond to bound states of the  $(A+1)$ -nucleus with excitation energy

$$E_x^{(A+1)} = \omega_k - \varepsilon_F^+, \quad (\text{B10})$$

see Eq. (B4).

Let us illustrate this description with two examples. In the case of neutrons in  $^{208}\text{Pb}$  one has

$$\begin{aligned} \varepsilon_t^+ &= 2.40 \text{ MeV}, & \varepsilon_t^- &= -14.09 \text{ MeV}, \\ \varepsilon_F^+ &= -4.03 \text{ MeV}, & \varepsilon_F^- &= -7.27 \text{ MeV}. \end{aligned} \quad (\text{B11})$$

In the case of the neutrons of  $^{10}\text{Be}$  one has

$$\begin{aligned}\varepsilon_t^+ &= 3.48\text{MeV}, & \varepsilon_t^- &= -8.48\text{MeV}, \\ \varepsilon_F^+ &= -0.50\text{MeV}, & \varepsilon_F^- &= -6.82\text{MeV}.\end{aligned}\tag{B12}$$

Of notice that when dealing with molecular systems, the quantities  $\varepsilon_F^-$  and  $\varepsilon_F^+$  are referred to as Highest Occupied Molecular Orbital (HOMO) and Lowest Unoccupied Molecular Orbital (LUMO).

While in the nuclear case, the prescription (see discussion following Eq. (B5))

$$\varepsilon_F = \frac{1}{2}(\varepsilon_F^+ + \varepsilon_F^-),\tag{B13}$$

has been used for closed shell nuclei [38] (e.g.  $\varepsilon_F(^{208}\text{Pb}) = -5.6\text{ MeV}$ ,  $\varepsilon_F(^{10}\text{Be}) = -3.7\text{ MeV}$ ), a more satisfying definition exists. In particular when studying nuclear superfluidity. In this case the BCS variational (Lagrange) multiplier used to fix the average number of nucleons, and usually denoted  $\lambda$ , is the chemical potential of the system (Fermi level) which in this case is equal to the Fermi energy  $\varepsilon_F$ .

It can be shown that  $\lambda/\hbar = \dot{\varphi}$ ,  $\varphi = i\partial/\partial N$  being the variable conjugated to the particle number operator  $\hat{N} = \sum_{\nu} a_{\nu}^{\dagger} a_{\nu}$ , while  $\dot{\varphi}$  is the rotational frequency in gauge space of the (ground state) pairing rotational band associated with gauge symmetry restoration (Anderson-Nambu-Goldstone mode, see [1] Ch. 4, and refs. therein). In keeping with the fact that gauge symmetry breaking is intimately correlated with the mixing of occupied ( $i$ ) and empty ( $k$ ) states, i.e. with particle number violation, and that a rotation can be viewed as large amplitude vibration in which the restoring force goes to zero while inertia remains finite, particle number (gauge) symmetry restoration implies  $W_1(\beta = +2) = W_1(\beta = -2) = 0$ . Making use of this prescription one obtains  $\varepsilon_F = -5.8\text{ MeV}$  and  $\varepsilon_F = -4.0\text{ MeV}$ , for  $^{208}\text{Pb}$  and  $^{10}\text{Be}$  respectively (minimum of the dispersion relation, see Fig. 5 of ref. [18] and Fig 23).

In a mean field approximation the energy of the last occupied single-particle level measured with respect to the continuum gives the nucleon separation energy. That is, the energy needed for promoting a bound nucleon into the lowest state of the continuum, the difference between the binding energy of a given nucleus and of its nearest neighbor. In other words, the energy gained adding (or removing) a nucleon.

In the case of  $^{208}\text{Pb}$  the mean field definition of the neutron separation energy  $S_n$  is the energy needed to take a neutron moving in the last occupied  $p_{1/2}$  orbit and bring it to

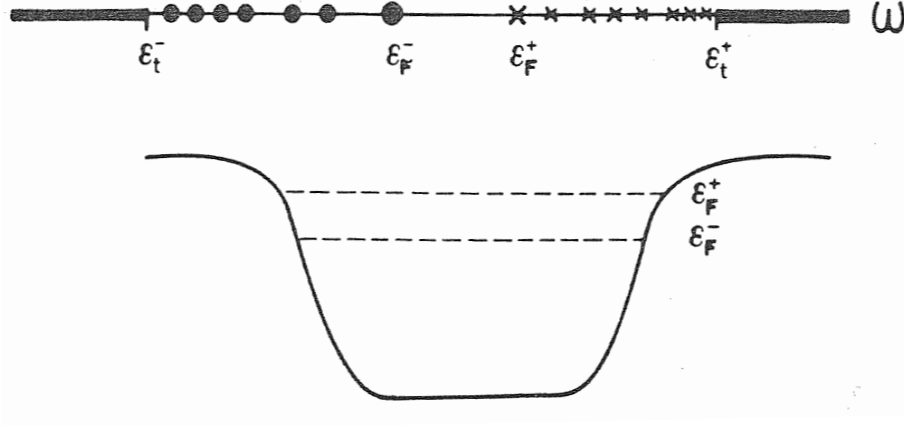


Figure 25. Schematic representation of the singularities of the one-body Green function  $G(\vec{r}, \vec{r}', \omega)$  in the complex  $\omega$ -plane.

become barely unbound. In other words, it is the energy of the  $p_{1/2}$  state with respect to the continuum, i.e.  $S_n(^{207}\text{Pb}) = 6.737$  MeV. Now the difference of binding energy between  $^{208}\text{Pb}$  and  $^{207}\text{Pb}$  measures the energy that is gained by adding a neutron to  $^{207}\text{Pb}$ , that is  $BE(^{208}\text{Pb}) - BE(^{207}\text{Pb}) = 7.27$  MeV. In the case of  $^{10}\text{Be}$  the mean field approximation neutron separation energy is  $S_n(^9\text{Be}) = 1.665$  MeV while  $BE(^{10}\text{Be}) - BE(^9\text{Be}) = 6.81$  MeV. These results testify to the fact that a pure mean field description of nuclei at large, and of  $^{10}\text{Be}$  and  $^{208}\text{Pb}$  in particular, is insufficient to account for all the effects defining the ground state of the system and that a more complete description is needed.

### Appendix C: The Copenhagen-Buenos Aires-Milan Nuclear Field Theory program

Let us elaborate on this need expressed making use of the  $N = 6$  shell closure, associated with the so called parity-inversion phenomenon, of which isotones  $^9\text{Li}$  and  $^{10}\text{Be}$  constitute paradigmatic embodiments. Within the framework of NFT, parity-inversion is associated with the inordinately large state dependent dressing of the  $1p_{1/2}$  and  $2s_{1/2}$  Saxon-Woods orbitals (to which a starting  $k$ -mass  $\approx 0.7m$  has been adscribed, see e.g. [8, 9] in keeping with the low density of the fermion system under consideration) describing the motion of a neutron around the core  $^9\text{Li}$  ( $^{10}\text{Li}$  resonant states) and  $^{10}\text{Be}$  ( $^{11}\text{Be}$  bound states) (see diagrams (a) and (b) inset of Fig. 10). In other words, the self-energy corrections described by these diagrams eventually propagated to all orders of perturbation (and which can be

parametrized in terms of the  $m_\omega$  effective mass) lead, in the case of  $^{10}\text{Li}$  and  $^{11}\text{Be}$ , to energy shifts larger than ever seen in systems lying along the stability valley with one nucleon on top of a closed shell system (see e.g.  $^{209}\text{Bi}$  and  $^{209}\text{Pb}$  [15, 54–56] and refs. therein). In keeping with this fact it is then only natural that the associated spectroscopic amplitudes ( $Z_\omega = (m_\omega/m)^{-1}$ ) are quite far from the single-particle values, and that the interaction between two nucleons surrounded by a cloud of e.g. dipole pigmy resonances, leads to a Cooper pair which is so extended as to make the  $^{11}\text{Li}$  radius about as large as 2/3 of the  $^{208}\text{Pb}$  radius. Now, this (halo) Cooper pair is the pair addition pairing vibrational mode of  $^9\text{Li}$ . Because this "object" is so fragile, and at variance with for example  $|^{210}\text{Pb}(gs)\rangle$ , a spectator, e.g. the pair removal mode of  $^9\text{Li}$ , i.e.  $|gs(^7\text{Li})\rangle$ , or the presence of a two-phonon p-h state (see Fig. 9(c)), can strongly perturb it. This is again at variance with what one observes in connection with the two-phonon, 4.9 MeV pairing vibrational mode of  $^{208}\text{Pb}$  (see [4, 18] and refs. therein).

Summing up, the strongly renormalized  $^{10}\text{Li}$  and  $^{11}\text{Be}$  single-particle states, i.e. dressed nucleons displaying effective  $\omega$ -masses and spectroscopic factors  $Z_\omega = (m_\omega/m)^{-1}$  very different from those of the original single-particle levels associated with the "bare" potential, interact among them, when moving in time reversal states, also very differently than bare nucleons do. Halos are just but a manifestation of this extreme interweaving of single-particle and collective motion which is at the basis of the structure of nuclei and which, in the present case, actually changes the very nature of the original Mayer and Jensen model [57], starting by the magic numbers, let alone the occupation numbers. This is because, as observed by Bohr and Mottelson [14, 25, 51, 58] the distribution of single-particle levels of the mean field which determines, in first approximation, the motion of nucleons, emerge from exactly the same nuclear properties which determine the collective motion of the nucleus as a whole. In fact, in a sense, the most collective nuclear motion is associated with the fact that a nucleon at the Fermi energy moves essentially independent of the rest of the other nucleons (long mean free path as compared to the nuclear radius), feeling their pushing or pulling only when trying to leave the nucleus, and being forced to bounce elastically off the nuclear surface.

A consequence of this fact, among other things, is that the distribution of valence orbitals around the Fermi energy determines the particle-hole excitations which are at the basis of e.g. collective surface vibrations. Thus, the fact that low-lying modes are, as a rule, of

quadrupole and octupole nature, as well as the associated spontaneous symmetry breaking phenomena (quadrupole and octupole rotational bands). The associated zero point motion can modify most of the nuclear properties, like the mean square radius (see e.g. [59, 60] and refs. therein), as well as the position and occupation of single-particle levels. In extreme cases, like the ones discussed above, even the magic numbers. Of notice that this is a dynamic Jahn-Teller type of effect, the one most commonly observed being the effect associated with the (static) phenomenon of spontaneous symmetry breaking in which the restoring force of, for example, a quadrupole vibration vanishes, its inertia remaining finite. The fingerprints of such phenomena are important rearrangements of single-particle levels (Nilsson potential [61]), and the presence of rotational bands with enhanced quadrupole transitions.

These effects can be so extreme in heavy nuclei that they lead e.g. to the phenomenon of exotic decay, the first observed case being that of  $^{223}\text{Ra} \rightarrow ^{209}\text{Pb} + ^{14}\text{C}$  (see e.g. [1] Ch. 7 and refs. therein), as extreme as the fact that  $^{11}\text{Li}$  is only marginally bound even if it is associated with a Mayer and Jensen magic number ( $N = 8$ ), magic number which because of the strong polarizability of the system (quadrupole vibration and pigmy resonance), shifts dynamically levels around leading to parity inversion and transforming  $^{11}_3\text{Li}_8$  from a single-closed shell system, into the exotic, halo, single Cooper pair weakly bound systems by the exchange of vibrations as recently experimentally demonstrated (see e.g. [26, 34, 62]), pair addition mode of the  $N = 6$  neutron closed shell.

Summing up, the Mayer and Jensen (independent particle) shell model [57], and the liquid drop model [63] are just two extreme aspects of the dynamical shell model (see e.g. [38] and refs. therein) in which the observed nuclear properties emerge from the interweaving (dynamical and static) of single-particle and collective degrees of freedom.

This scenario is at the basis of the Bohr-Mottelson model. Within this context, the systematic use of NFT to work out the variety of couplings and processes dressing nucleons and collective modes (Feynman-Goldstone-like diagrams as well as Bès-BRST) provides the theoretical framework to carry, arguably, the Copenhagen-Buenos Aires-Milan program (for both structure [10–16, 58, 64] and reactions [17]) to completion, renormalizing not only the elementary modes of excitation, but also their interactions, effective operators and related scattering processes and probes.

The extreme consequences of such renormalizations observed in e.g. the nuclei  $^{10}\text{Li}$ ,  $^{11}\text{Li}$ ,  $^{11}\text{Be}$ ,  $^{12}\text{Be}$ , force one to recognize that such a program is not an option, but that it is a



prerequisite to be able to compare quantitatively theory with experiment.

## Appendix D: Nuclear Reactions

### *c. Elastic scattering*

Consider an incident beam of particles of mass  $m$  moving along the  $z$ -axis with a velocity  $v$  and impinging on a scattering center. Such a system can be described in terms of a plane wave

$$\Psi_{inc} = \Psi_{\alpha} e^{ikz}, \quad (D1)$$

where  $k = mv/\hbar$ ,  $v$  being the velocity corresponding to the incident projectile energy, while  $\Psi_{\alpha}$  describes the intrinsic structure of the incoming particles along the  $z$ -axis. the associated incident current can be determined from the relation

$$\vec{I} = \frac{\hbar}{2im} (\Psi^* \vec{\nabla} \Psi - (\vec{\nabla} \Psi^*) \Psi) = \Im m \{ \Psi^* \vec{\nabla} \Psi \}, \quad (D2)$$

leading to

$$\vec{I}_{inc} = |\Psi_{\alpha}|^2 v \hat{z}. \quad (D3)$$

The scattering center interacts with the incident particles to produce an outgoing (elastic) scattering (spherical) wave, with axial symmetry with respect to the incident beam. At a large distance from the scatter this wave has the form

$$\Psi_{scatt} = \Psi_{\alpha} f(\theta) \frac{e^{ikr}}{r}. \quad (D4)$$

The associated scattered current is equal to

$$\vec{I}_{scatt} = |\Psi_{\alpha}|^2 v \frac{|f(\theta)|^2}{r^2} \hat{r} \quad (D5)$$

The flux outgoing particles is given by the projection of  $\vec{I}_{scatt}$  on the unit area  $d\vec{A}$  parallel to  $\hat{r}$ , that is,

$$\vec{I}_{scatt} \cdot d\vec{A} = |\Psi_{\alpha}|^2 v \frac{dA}{r^2}. \quad (D6)$$

It is of notice that  $\frac{d\vec{A}}{r^2} = d\Omega \hat{r}$  where  $d\Omega$  is the unit of solid angle, thus

$$\vec{I}_{scatt} \cdot d\vec{A} = |\Psi_{\alpha}|^2 v d\Omega. \quad (D7)$$

The differential cross section is defined as the scattered flux divided by the incoming flux, namely,

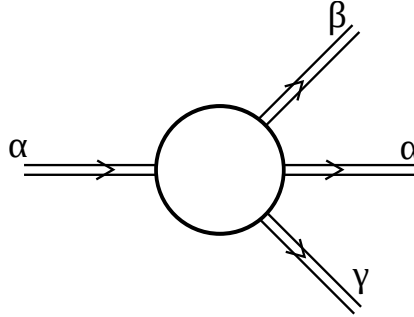
$$d\sigma = \frac{\vec{I}_{scatt} \cdot d\vec{A}}{\vec{I}_{inc} \cdot \hat{z}} = |f(\theta)|^2 d\Omega, \quad (D8)$$

and

$$\frac{d\sigma}{d\Omega} = |f(\theta)|^2 \quad (D9)$$

*d. Inelastic and transfer reactions*

Let us consider the reaction  $A(a, b)B$ , where  $\alpha = a + A$  and  $\beta = b + B$  label the elastic and a general inelastic or transfer channel respectively. The wavefunction describing the



above process can be written as

$$\Psi = e^{i\vec{k}_\alpha \cdot \vec{r}_\alpha} \Psi_a(\xi_a) \Psi_A(\xi_A) + \sum_\beta \Psi_{scatt, \beta} \quad (D10)$$

where  $\Psi_a(\xi_a)$  and  $\Psi_A(\xi_A)$  are the intrinsic wavefunctions in channel  $\alpha$  ( $\int |\Psi_a(\xi_a)|^2 d\xi_a = \int |\Psi_A(\xi_A)|^2 d\xi_A = 1$ ) while

$$\Psi_{scatt, \beta} = f_\beta(\theta) \frac{e^{ik_\beta r_\beta}}{r_\beta} \Psi_b(\xi_b) \Psi_B(\xi_B), \quad (D11)$$

with  $\int |\Psi_b(\xi_b)|^2 d\xi_b = \int |\Psi_B(\xi_B)|^2 d\xi_B = 1$ .

In analogy with the elastic process, one can define the reaction differential cross section  $d\sigma_{\alpha \rightarrow \beta}$  as

$$d\sigma_{\alpha \rightarrow \beta} = \frac{v_\beta |f_{\alpha \rightarrow \beta}(\theta)|^2}{v_\alpha} d\Omega, \quad (D12)$$

that is,

$$\frac{d\sigma_{\alpha \rightarrow \beta}}{d\Omega} = \frac{v_\beta}{v_\alpha} |f_{\alpha \rightarrow \beta}(\theta)|^2. \quad (D13)$$

For elastic scattering we have  $v_\alpha = v_\beta$ . When the scattering is non-elastic, the factor  $(v_\alpha/v_\beta)$  enters because the cross section refers to particle flux whereas the wave amplitude  $f$  describe particle density.

*e. Detailed Balance*

Of course

$$|f_{\alpha \rightarrow \beta}(\theta)|^2 = |f_{\beta \rightarrow \alpha}(\theta)|^2, \quad (\text{D14})$$

in keeping with detailed balance. However, the corresponding cross sections may be very different. For example in the case of the reaction at  $E_{11\text{Li}} = 33$  MeV ( $E_{CM} = 2.75$  MeV)

$$^{11}\text{Li}(p, t)^9\text{Li}(gs), \quad (\text{D15})$$

where the total cross section is  $\sigma \approx 6\text{mb}$ ,  $(v_\beta/v_\alpha) = v_{9\text{Li}-t}/v_{11\text{Li}-p} \approx 3$ . Consequently, the inverse reaction  $^9\text{Li}(t, p)^{11}\text{Li}(gs)$  (for which  $k_i = 0.347 \text{ fm}^{-1}$  and  $k_f = 1.085 \text{ fm}^{-1}$ ) at identical bombarding conditions in the center of mass system is predicted to display a total cross section of  $\approx 0.6 \text{ mb}$  (see Fig. 26).

## Appendix E: Correlation length and Cooper pair transfer

The two halo neutrons in  $^{11}\text{Li}$  have a separation energy of about 380 keV. Consequently, one can consider this system as a textbook example to study the nuclear embodiment of a Cooper pair, namely two-fermions on top of a Fermi sphere with which it communicates solely in terms of the Pauli principle, all other possible medium polarization effect being included in the strongly renormalized interaction acting among the pair partners (within this context see [65]). Making use of the fact that the observed mean square radius of  $^{11}\text{Li}$  is  $\langle r^2 \rangle^{1/2} = 3.55 \pm 0.1 \text{ fm}$  and that  $R \approx (5/3)^{1/2} \langle r^2 \rangle^{1/2}$ , one can argue that, making use of the parametrization  $R = r_0 A^{1/3}$ , with  $r_0 = 1.2 \text{ fm}$ , for the nuclear radius, the exotic  $^{11}\text{Li}$  nucleus behaves as a normal system lying along the stability valley of mass number  $A \approx 60$ , i.e. a nucleus displaying a radius of 4.6 fm, to be compared with that of  $^9\text{Li}$ ,  $R = 1.2 \times 9^{1/3} \text{ fm} \approx 2.5 \text{ fm}$ .

While one cannot produce a chunk of matter made out of  $^{11}\text{Li}$  separated by about two nuclear diffusivities ( $2a \approx 1.6 \text{ fm}$ ), and thus observe neutron supercurrents (nuclear superfluidity), as it is possible in the case of e.g. alkali doped  $C_{60}$  fullerenes, namely Van der Waals

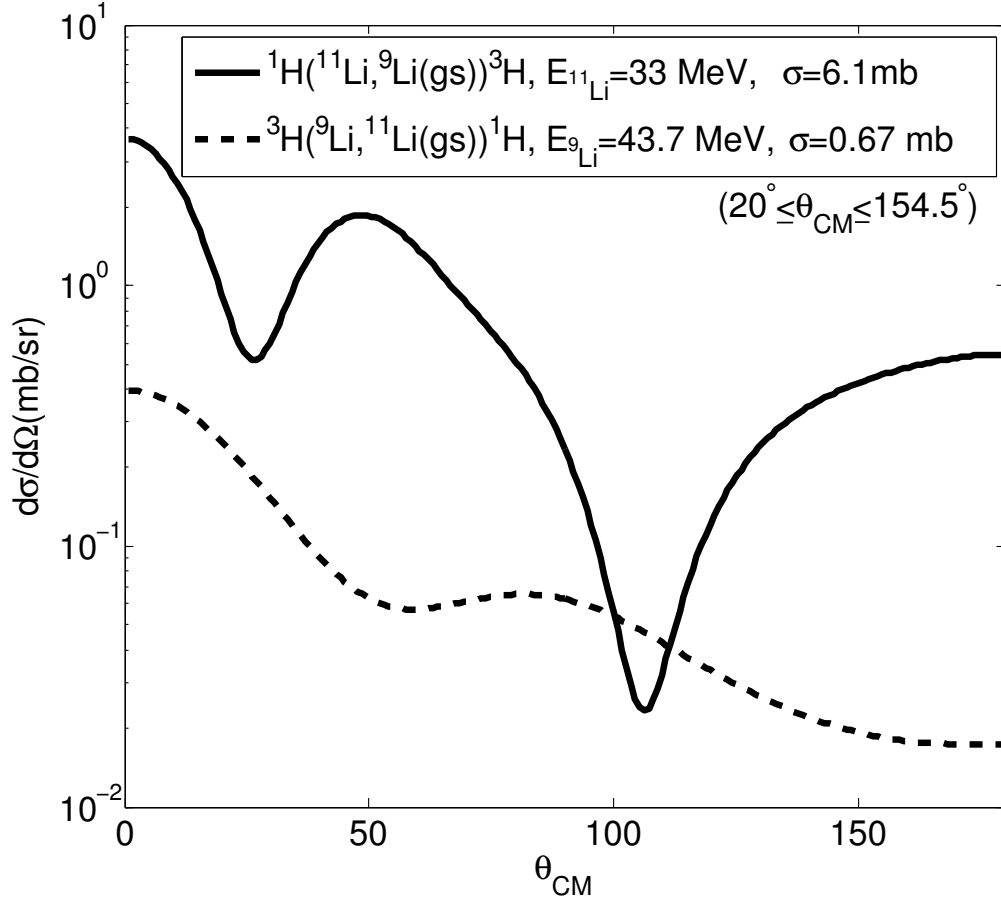


Figure 26. Two nucleon transfer reaction on Lithium with inverse kinematics: (continuous curve), absolute differential cross section for the reaction  ${}^1\text{H}({}^{11}\text{Li}, {}^9\text{Li}(gs)){}^3\text{H}$  at a bombarding energy of  $E_{11\text{Li}} = 33$  MeV ( $Q = 8.18$  MeV) corresponding to a center of mass energy of  $E_{CM} = 2.75$  MeV; (dashed curve)  ${}^3\text{H}({}^9\text{Li}, {}^{11}\text{Li}(gs)){}^1\text{H}$  at a  ${}^9\text{Li}$  bombarding energy of  $E_{9\text{Li}} = 43.7$  MeV ( $E_{CM} = 10.93$  MeV).

solids (cf. [66–71] and refs. therein), it is in principle conceivable to study the Cooper pair tunneling in which the partner neutrons are correlated over a distance of 20 fm. This is, in principle, to be done with the help of the  ${}^{11}\text{Li} + {}^{11}\text{Li}$  reaction. From the associated differential cross section of pair tunneling, and thus the building blocks of (neutron) superflow in a *gedanken* non-overlapping  ${}^{11}\text{Li}$  solid (of unit cell as shown in Fig. 27), namely (hopping) pair tunneling, one may estimate how large the contribution to it arises from situations in which tunneling takes place when the halo neutrons are separated by a full correlation length ( $\xi \approx 20$  fm), as schematically shown in Fig. 27.

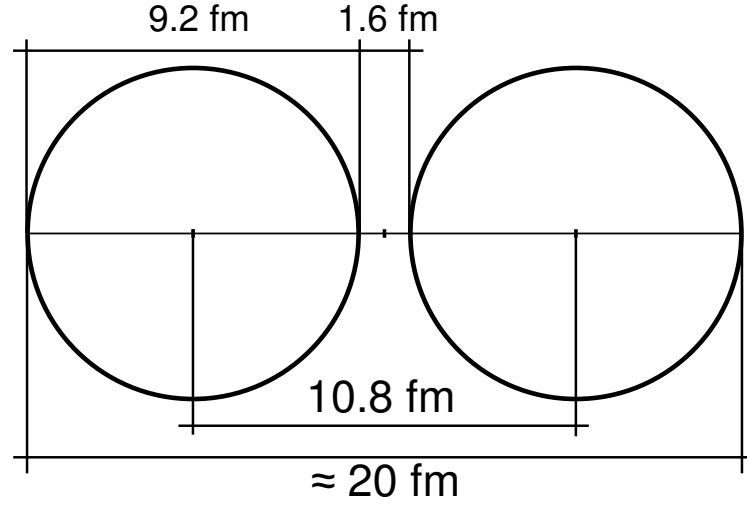


Figure 27. Schematic representation of the distance of closest approach configuration of a two-particle transfer process in the reaction  $^{11}\text{Li} + ^{11}\text{Li}$  at distances of the order of  $2(R + a)$ , where  $a$  is a length of the order of the  $^{11}\text{Li}$  nuclear diffusivity. For distances smaller than this distance, absorption will essentially depopulate any particular direct channel, e.g. two-particle transfer channel. At distances considerably larger, the two-particle transfer formfactor will be too small to lead to measurable transfer cross sections. Thus, one can assume that  $2a$  is the optimal surface-surface relative distance for Cooper pair tunneling.